Exo-Abs: A Wearable Robotic System Inspired by Human Abdominal Muscles for Noninvasive and Effort-Synchronized Respiratory Assistance

Sang-Yoep Lee, *Member, IEEE*, Jin-Oh Hahn, *Senior Member, IEEE*, Jaewon Beom, Ji-Hong Park, Han Eol Cho, Seong-Woong Kang, and Kyu-Jin Cho, *Member, IEEE*

***Abstract*—Existing technologies for patients with respiratory insufficiency have focused on providing reliable assistance in their breathing. However, the need for assistance in other everyday respiratory functions, such as coughing and speaking, has remained unmet in these patients. Here, we propose Exo-Abs, a wearable robotic system that can universally assist wide-ranging respiratory functions by applying compensatory force to a user's abdomen in synchronization with their air usage. Inspired by how human abdominal muscles transmit pressure to the lungs via abdominal cavity compression, a biomechanically interactive platform was developed to optimally utilize the abdominal compression while aligning the assistance with a user's spontaneous respiratory effort. In addition to the compact form factor, thorough analytic procedures are described as initial steps toward taking the human respiratory system into the scope of robotics technology. We demonstrate the validity of the overall human–system interaction with the assistance performance under three essential respiratory functions: breathing, coughing, and speaking. Our results show that the system can significantly improve the performance of all these functions by granting on-demand and self-reliant assistance to its users.**

***Index Terms*—Assistive technology, biologically inspired robots, biomedical engineering, human–robot augmentation, physical human–robot interaction, rehabilitation robotics.**

Manuscript received September 26, 2021; revised February 18, 2022; accepted March 8, 2022. This work was supported in part by the National Research Foundation of Korea Grant funded by the Korean Government under Grant NRF-2016R1A5A1938472 and in part by the U.S. Office of Naval Research under Grant N00014-19-1-2402. This article was recommended for publication by Associate Editor F. Ficuciello and Editor A. Menciassi upon evaluation of the reviewers' comments. *(Corresponding author: Kyu-Jin Cho.)*

Sang-Yoep Lee and Kyu-Jin Cho are with the Biorobotics Laboratory, Department of Mechanical Engineering, SNU-IAMD, Institute of Engineering, Soft Robotics Research Center, Seoul National University, Seoul 08826, South Korea (e-mail: wsheaven@snu.ac.kr; kjcho@snu.ac.kr).

Jin-Oh Hahn is with the Department of Mechanical Engineering, University of Maryland, College Park, MD 20742 USA (e-mail: jhahn12@umd.edu).

Jaewon Beom and Ji-Hong Park are with the Department of Rehabilitation Medicine, Seoul National University College of Medicine, Seoul National University Bundang Hospital, Seongnam 13620, South Korea (e-mail: powe5@snubh.org; wpeo00@gmail.com).

Han Eol Cho and Seong-Woong Kang are with the Department of Rehabilitation Medicine, Gangnam Severance Hospital, Rehabilitation Institute of Neuromuscular Disease, Yonsei University College of Medicine, Seoul 06273, South Korea (e-mail: wtzephyr@yuhs.ac; kswoong@yuhs.ac).

This article has supplementary material provided by the authors and color versions of one or more figures available at https://doi.org/10.1109/TRO.2022.3167399.

Digital Object Identifier 10.1109/TRO.2022.3167399

NOMENCLATURE

T	Tension in the belt-based pressure transmission assembly.
τ_{motor}	Motor torque.
r_0	Radius of the shaft in the belt-wrapping mechanism.
w	Thickness of the actuation belt in the belt-wrapping mechanism.
θ_{motor}	Angular displacement of the motor.
F^i	Force applied on the *i*th subdivided abdominal wall.
φ_{abs}	User-dependent constant for configuration of wearing Exo-Abs; angle between two lines connecting the origin of the cross-sectional ellipse of a user's abdominal cavity and belt contact points.
x	Hypothetical displacement to represent deformation in the abdominal cavity.
F	Net force applied on the abdominal wall.
a, b	Semi-major and semi-minor axis of an ellipse that models cross-sectional contour of a user's abdominal cavity.
m, c, k	Lumped inertia, damping, and stiffness of the abdominal cavity.
h	Equivalent height of an elliptic pillar for expressing volume in the abdominal cavity.
V_{ab}, P_{ab}	Volume and pressure in the abdominal cavity, respectively.
γ	Heuristic gain parameter for adjusting the ratio between the abdominal cavity compression and the pressure increase in the lung.
$R,\ E$	Airway resistance and lung elasticity.
V_{lung}	Air volume in the lungs.
P^{mus}	Pressure in the lungs generated by human respiratory muscles.
P^{exo}	Additional pressure in the lungs generated by Exo-Abs.
P^{PEEP}	Positive-end expiratory pressure in the lungs.
V^0_{lung}	Residual lung volume.
P^{exo}_{ref}	Proposed control policy.
$k_R,\ k_E$	Gain parameters of the resilient context-aware control.
$k_P,\ k_D$	Gain parameters of the proportional-derivative control for the abdominal cavity compression.

I. Introduction

THE ability to control the amount and rate of volume change in the lungs is one of the most essential functions in humans, in that it not only enables breathing but also facilitates various everyday respiratory functions such as coughing and speaking [1], [2]. Thus, one may experience a substantial deterioration in both health and quality of life when their respiratory muscles are weakened due to a neurological injury or disease [3]. The majority of these patients require assistance in various everyday respiratory functions even if they do not show severe symptoms such as respiratory failure [4], [5]. Insufficient coughing ability increases the risk of pneumonia, whereas shortened breathing limits their ability to communicate. However, the need for such assistance often remains unmet in patients with relatively mild respiratory dysfunctions. Indeed, existing mechanical ventilators and cough-assist machines are not suitable for all-day assistance that allows users to engage in routine social activities. Moreover, these devices make the patients dependent on caregivers for everyday tasks and add hygiene-related burden on the users [6]–[8].

For patients suffering from chronic respiratory insufficiency, noninvasive positive pressure ventilators (NIPPVs) are the most common solution for portable and prolonged assistance in current clinical practice [9]. NIPPVs can precisely control the amount of air inhaled and exhaled by the user through a ventilation mask. Despite their reliability, NIPPVs necessitate continuous airway intervention that prevents the user from performing respiratory functions other than rhythmic breathing [10], [11]. Ventilation masks also have issues that limit their use in patients [12]. NIPPVs cannot be applied if the ventilation mask does not fit a user's face shape or causes panic disorder. Skin irritation from prolonged contact with the ventilation mask is another limiting factor. As an alternative, body ventilators (BVs) were introduced in place of NIPPVs in such patients. BVs apply either positive or negative pressure to the body to generate a pressure difference between the lungs and atmosphere [13]. Although BVs can alleviate the discomfort caused by the use of ventilation masks, most BVs are associated with a number of drawbacks: they are 1) open-loop controlled, 2) asynchronous with the user's respiratory effort, and 3) cannot assist various respiratory functions. Therefore, the use of BVs is limited to the attenuation of irregular residual lung volume of patients even when the patients can actively adapt to the BVs [14].

To address such challenges in biomechanical interaction, recent advances in wearable robotic technologies provide physiological and nonrestrictive assistance in everyday human activities by utilizing compliant materials such as fabrics and elastomers [15]–[18]. For instance, the authors in [16] and [17] demonstrated that a soft wearable robot constructed using textile anchors and cable-based transmissions could effectively assist patients with neurological injuries during walking and grasping tasks. These unobtrusive robotic components may likewise be utilized to compensate for insufficient respiratory ability while avoiding unwanted interference with other body parts, in a way that is much more physiologically viable than mechanical ventilators [11], [19]. Nevertheless, a more elaborate and sophisticated design effort is required to realize wearable robotic respiratory assistance. State-of-the-art wearable robotic technologies tend to exert mechanical power transmission directly on body parts [20], [21]. In contrast, it is not easy to interact directly with the lungs because they are enclosed in complex anatomical surroundings such as the ribcage and diaphragm.

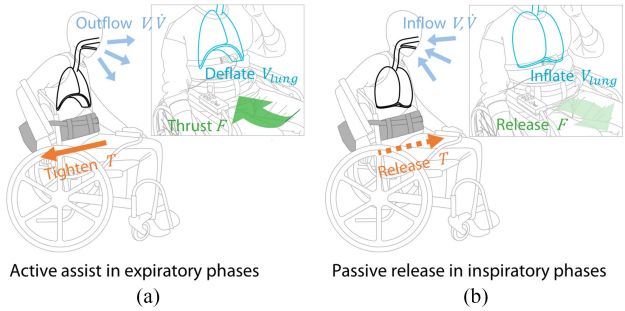

Fig. 1. Concept of the proposed respiratory assistance with Exo-Abs. (a) System applies compressive force in the expiratory phases and (b) releases it in the inspiratory states. The terms written aside are described in detail in the nomenclature below.

The abdominal muscles in the body elucidate an inspiring strategy to engage in controlling volume in the lungs. These outermost muscles transmit a large pressure with no direct interaction with the airway by effectively compressing the abdominal cavity. This is possible with the unique characteristics related to abdominal wall contraction that presents a fundamentally different perspective from how human skeletal muscles have inspired engineers: typical articulatory muscles reduce their length to generate force, whereas the abdominal muscles reduce their area to generate pressure distribution. Furthermore, the abdominal muscles have three important anatomical features that contribute to the effective volume change in the abdominal cavity. First, they compactly cover the abdominal cavity and compress it radially inward [22], [23]. Second, the muscles, especially the *external oblique muscle*, lead the wall movement upward and project more pressure to the diaphragm [24]. Third, the effective stiffness of the abdominal wall increases as the muscles contract, distributing pressure evenly within the surface [25], [26]. Hence, the abdominal muscles provide a multifaceted perspective to design an efficient biomechanical system for respiratory interaction.

Here, we propose Exo-Abs, a wearable robotic system that can resiliently apply compensatory force to a user's abdomen in synchronization with their air usage context [27], [28] (Fig. 1). To design a system that can serve as a supplementary respiratory muscle applicable universally to a wide spectrum of respiratory functions, synchronization with a user's respiratory effort is essential. We present two novel ideas to realize robust synchronization. First, a belt-based pressure transmission assembly is proposed for real-time user–system interaction with fast actuation-to-airflow response time. The three anatomical features of the abdominal muscles provide insights to generate

isotropic volume change in the abdominal cavity. This design approach allows the belt assembly to evenly distribute the compressive force within the abdominal wall and to project more pressure to the lungs, thereby enabling the system to assist even fast respiratory functions such as coughing [29]. Second, a resilient context-aware control scheme is developed to tailor the robotic actuation to a wide spectrum of respiratory functions from calm breathing to coughing and speaking. A customized spirometer, chest-belt plethysmograph, and microphone were employed to monitor the user's air usage context and respiratory effort. Capitalizing on these sensors, the system can adjust the intensity, speed, and timing of the actuation [30], [31], while satisfying the safety criteria [6], [8], [9] and rejecting various disturbances from the user's posture and clothing.

We experimentally demonstrate the ability of the system to assist a user in three important everyday respiratory functions: breathing, coughing, and speaking. These three functions were chosen as essential respiratory functions that present challenges to patients with neurological disorders in their everyday lives [3]. Experiments were conducted to validate the proof-of-concept of the user–system synchronization and to compare the performance of these respiratory functions with and without the robotic assistance. One healthy participant and nine patients with various neurological disorders were recruited to test the applicability of the system to users with diverse physiological characteristics. With detailed results obtained under practical use scenarios, we demonstrate three important robotic contributions. First, the analytic procedures provided a novel idea to enable robotic interaction with biomechanics that does not incorporate clear link-and-joint structures. Second, the compact form factor realized with the soft wearable robotic technology suggested the potential to expand the application of respiratory assistance and rehabilitation toward a wider user group. Third, Exo-Abs served as a robotic tool to investigate the dynamics of human respiration subject to external abdominal compression, which has not been analytically and quantitatively studied so far.

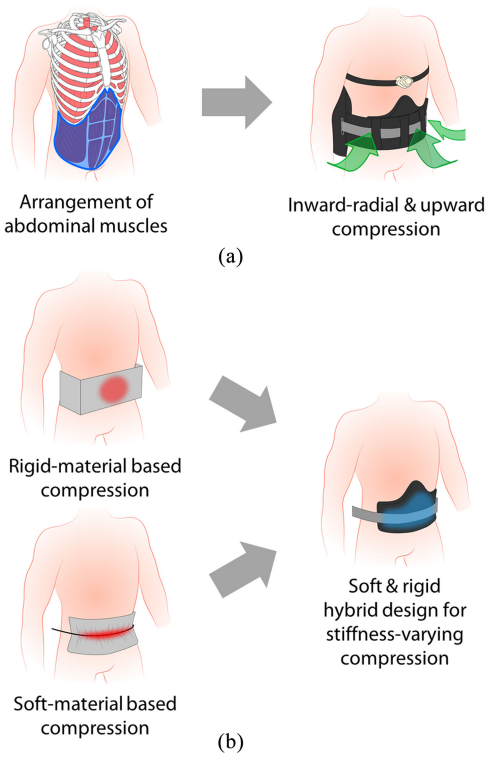

Fig. 2. Bioinspired design of the belt-based pressure transmission assembly. (a) Inspired by the arrangement of the abdominal muscles, the belt assembly compactly covers the abdominal cavity while reconciling complex anatomical surroundings. (b) Inspired by the stiffness characteristics of the abdominal muscles, the belt assembly conforms to the abdominal wall and produces an efficient volume change of the abdominal cavity while avoiding pressure concentration.

II. System Development

A. Design and Actuation of Belt-Based Pressure Transmission Assembly

The arrangement and stiffness characteristics of human abdominal muscles make it possible to increase the efficiency of pressure transmission and to avoid a force concentration to the intestine or bones. We designed a belt-based pressure transmission assembly to replicate these features in our robotic-assistive system (Fig. 2). The belt assembly consists of a router belt, an actuation belt, and a set of cushioning pouches (Fig. 3). The router belt holds both the actuation belt and the cushioning pouches, and secures them against disturbances such as clothing displacement and body movement. The actuation belt transmits tension generated from the actuation system to the user's abdomen in the form of radially inward compressive force. Attached to the router belt, the cushioning pouches contain layers of pads with different stiffness characteristics; soft pads are placed facing the user to conform to the shape of the user's abdomen when the tension of the actuation belt is low, whereas rigid pads are placed facing the actuation belt to distribute the force from the actuation belt evenly to the user's abdomen when the tension of the actuation belt is high. Combined, these cushioning pouches work as a component with varying stiffness depending on the tension of the actuation belt by continuously switching the main target of compression from the cushioning pouches to the user's abdomen. The stiffness characteristics of each cushioning pouch can be customized to a different user by changing its pad combination, and this "mechanical impedance matching" process facilitates the generalized analysis introduced in the following sections.

The actuation of the belt-based pressure transmission assembly is based on a belt-wrapping mechanism. The actuation belt passes through a slit in a steel shaft. After the two ends of the belt are buckled in front of the user's abdomen, the belt assembly compresses the abdomen of the user as the tension increases. The shaft is coupled to the main motor (EC-4pole, MAXON MOTOR AG). Because the deformation of the abdominal cavity is highly elastic over the range of the system's motion for assistance, a fast yet accurate force generation is required [32]. The maximum applicable net force integrated over a user's abdomen is 800 N, which is the maximum force level that can be delivered to patients for respiratory assistance. The electric

Fig. 3. Belt-based pressure transmission assembly. (a) Router belt and cushioning pouches. (b) Cushioning pouches contain layers of pads with different stiffness of each. (c) Belt assembly worn on a manikin.

TABLE I
DETAILED INFORMATION OF ABDOMINAL COMPRESSION PERFORMANCES WITH RESPECT TO DESIGN OF COMPRESSION COMPONENT

	Naïve design	Bioinspired design
Area	114 cm^2	300 cm^2
Net force	137.05 N	272.85 N
Distribution	12.02 $\pm$ 6.95 kPa	9.11 $\pm$ 3.32 kPa

The naïve convex design emulated manual abdominal compression that can be delivered by therapists.

components for the actuation consist of a custom-built battery pack, motor driver (ESCON 70/10, MAXON MOTOR AG), shunt regulator (Shunt Regulator DSR 70/30, MAXON MOTOR AG), voltage converter (120 W dc–dc converter 12 V/10 A, DFRobot), and custom circuitry containing other peripheral electrical elements. Other than the electric components, a load cell (333FDX—100kgf, KTOYO) combined with an analog load cell amplifier (Load Cell Amplifier PRO, ELANE) and an encoder (HEDL 5540, 500CPT, MAXON MOTOR AG) is installed for monitoring the abdominal cavity compression.

The improvement in the abdominal compression performance based on the bioinspired design was demonstrated by analyzing the pressure distribution between the pressure transmission assembly and the abdominal wall in comparison to a naïve competing design: a belt with a simple compression component that emulates the technique of manual abdominal thrust (which has been widely used in medical practice). A multigrid pressure mat (Pliance, Novel) was used to monitor the real-time pressure distribution. Under the same tension condition in the actuation belt, largely smaller standard deviation in the pressure measured in each grid was expected, which leads to an isotropic volume change in the abdominal cavity. As shown in Fig. 4 and Table I, the belt-based pressure transmission assembly was able to apply pressure with 163% increased compression area, 52% decreased standard deviation, and 99% increased force. The result indicates

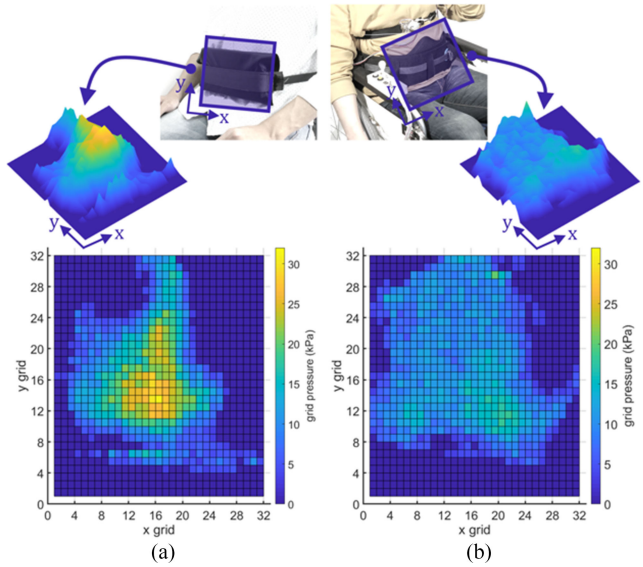

Fig. 4. Demonstration of pressure distribution performance associated with (a) simple naïvely designed pressure transmission assembly and (b) proposed belt-based pressure transmission assembly.

that the bioinspired design approach to the belt-based pressure transmission assembly could produce more efficient abdominal compression in each air usage.

B. Custom-Designed Spirometry and Plethysmography for Real-Time Respiratory Function Monitoring

To assist respiratory functions in humans, the system must measure the amount and rate of volume change in the lungs and use them to control its actuation. However, human lungs are difficult to monitor in real time without utilizing techniques such as computerized tomography or magnetic resonance imaging [9]. Here, two sensors were custom-designed as a more applicable alternative solution: a spirometer and a chest-belt-type plethysmograph. Both sensors were designed and optimized to reliably capture respiratory signals from the users while minimizing invasiveness, intense installation procedure, and disruption from their body motion [33].

For the spirometry, a modified Fleisch-tube type flowmeter was designed. Traditional Fleisch-tube includes capillary-like structures inside the tube to generate laminar flow. To facilitate manufacturing, the capillary-like structures were replaced by slit structures. The tube was fabricated using a three-dimensional printer (Objet 260 Connex, Stratasys) with a biocompatible material (VeroWhitePlus, Stratasys). The amount of airflow passing through the tube can be estimated using the differential pressure between two separate points of the tube. For sensing differential pressure in the tube, a pair of differential pressure sensors (SDP2000-L, SENSIRION) was used. The spirometer is able to sense airflow through the tube with a resolution of 3.1 ml/s.

For plethysmography, a draw-wire sensor that can be worn on a user's chest was fabricated. The chest perimeter was monitored and used as a proxy to estimate the user's lung volume over time.

Existing chest-belt type plethysmographs utilize inductance by embedding a coil on an elastic band, but they have the disadvantage of being vulnerable to electrical disturbances. Hence, we fabricated a mechanical-type sensor with a reel spring and an encoder (RM08, RLS). It is similar to a digital tape measure, but an elastic cord that matches the impedance of the expansion motion of the chest was used to adapt to various users without impeding respiration-related actions. The chest-belt plethysmograph must expand and recover promptly as the user inhales and exhales to accurately estimate the volume of the lungs from the circumference of the user's chest. Therefore, the stiffness of both the elastic cord connected to the chest belt and the reel spring in the plethysmograph was carefully chosen to ensure sensitivity while avoiding discomfort when worn.

In actual implementation, these sensors are utilized in a way that can prevent discomfort due to prolonged use by reconciling sensing accuracy with comfort. In particular, the spirometer can measure exact airflow in real time. Yet, it is not convenient for long-term use since it requires the use of a mouthpiece. The chest-belt plethysmograph is much more convenient, and it can detect and track the respiratory phases adequately. However, it requires intermittent calibrations to make up for disturbances in measurement conditions such as posture and clothing. Hence, a user can make personalized compromise between performance and comfort depending on their preference. For instance, one can use the system only with the plethysmograph to self-assist continued calm breathing during a downtime, while one can use both the spirometer and the plethysmograph during respiratory training to achieve accurate assistance pattern for rehabilitation.

In order to assess the performance of the Exo-Abs sensor combination, real-time measurements from Exo-Abs were compared with those from two commercial medical instruments—a sonograph (SONON 300L, HEALCERION) and a medical-grade spirometer (SP10, CONTEC MEDICAL SYSTEMS). First, sonography was employed to evaluate the phase-sensitiveness of the Exo-Abs sensor combination by analyzing the true lung images obtained in real time [Fig. 5(a)]. Since it is difficult to include the whole view of the lungs in every image, a fixed spot of a lung was monitored to track the motion of its rim [Fig. 5(b)]. Then, the time-series phase information of lung volume deviation was extracted from the sonograph images. After normalizing the time-series lung volume measurements from Exo-Abs that were simultaneously obtained with sonography, the overall phase difference could be calculated with the method based on discrete Fourier transform described in [34] and [35]. As shown in Fig. 5(c), $1.61 \cdot 10^{-4}$ radians of phase difference was calculated over the whole measurement. Second, the accuracy of the Exo-Abs sensor combination was evaluated by utilizing a medical-grade spirometer. Peak expiratory flow and tidal volume, which are standard measures used to quantify the lung function, were simultaneously obtained from both devices and compared. The error was bounded within $\pm 4\%$ for peak expiratory flow and $\pm 6\%$ for tidal volume [Fig. 5(d)]. All in all, the error was small to the extent that can be canceled out with the proposed control policy described in Section IV.

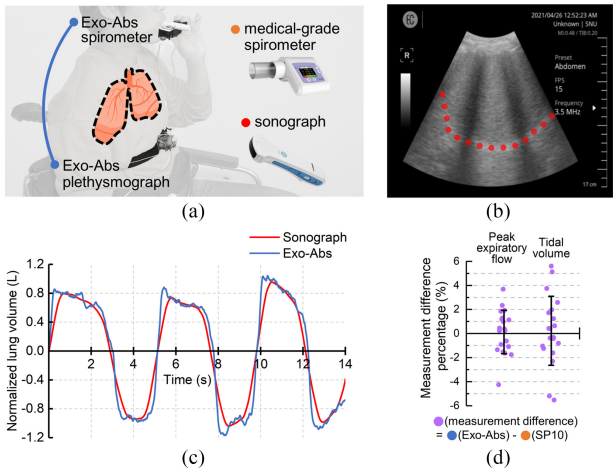

Fig. 5. Validation of the Exo-Abs sensor combination. (a) Schematic of the validation strategy. (b) Sonograph image with the rim of a lung marked with red points. (c) Simultaneous lung volume measurements with a sonography and Exo-Abs for comparing phase-sensitiveness. (d) Simultaneous air usage measurements with a commercial medical-grade spirometer and Exo-Abs for comparing accuracy.

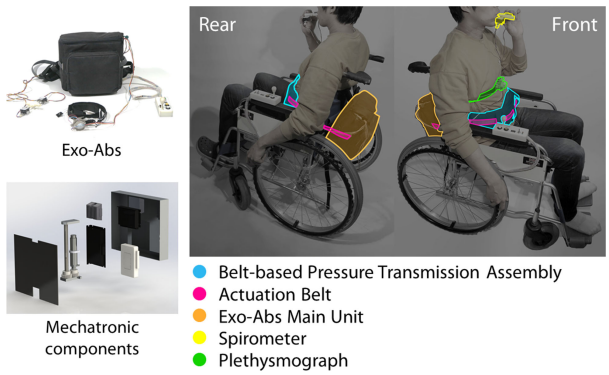

Fig. 6. Components of Exo-Abs. Main unit includes mechatronic components and the belt-wrapping mechanism.

C. Operational Interface and Control for Respiratory Assistance

Along with the belt-based pressure transmission assembly, a backpack was introduced to encase the overall system and to maintain the direction of the actuation belt upward [36]. Because many patients with neurological disorders use wheelchairs in their everyday lives, the backpack may be anchored to commonly used wheelchairs (Fig. 6). Alternatively, the system can be worn as a backpack (Fig. 7). Thanks to this form factor, the system can provide respiratory assistance without impeding the motion of other body parts.

In addition to the spirometer and the plethysmograph, a microphone (BFM294839, SHURE) was introduced to the operational interface for synchronizing the system's assistance to a user's respiratory effort in various respiratory functions (Fig. 8). The spirometer and the plethysmograph monitor the volumetric flow rate (VFR) and the moved air volume (MAV),

Fig. 7. Three possible configurations for the use of Exo-Abs. By virtue of the backpack design, the system can be worn in a highly versatile fashion, including (a) on the back of the body, (b) on a chair, (c) or on a wheelchair.

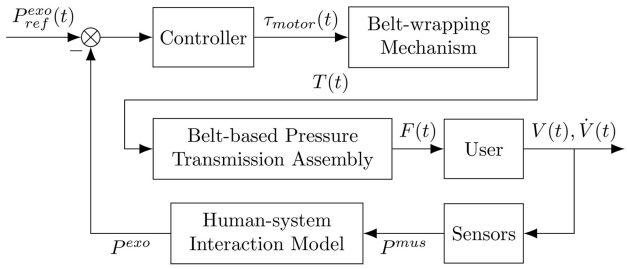

Fig. 9. Block diagram for the overall human–system interaction.

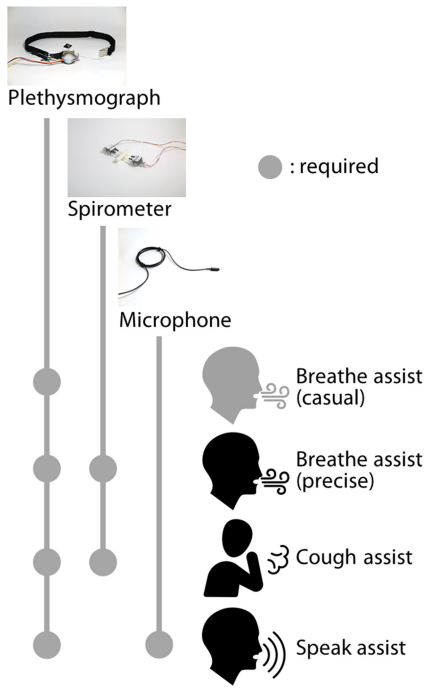

Fig. 8. Schematic representation of the resilient context-aware assistance. The chest-belt plethysmograph is required in every case to monitor the phase of air usage, avoiding asynchrony. The spirometer monitors direct air usage from the user, enabling the system to provide precise assistance informed by the VFR. If the spirometer detects a sudden large inhalation, the system interprets this as an intention of generating instantaneous large VFR and MAV such as coughing. If the microphone detects speech when the spirometer is not measuring airflow, the system interprets the situation as speaking and provides assistance.

while the microphone detects whether a user is speaking, and if so, measures the voice level as a proxy for VFR. Based on the respiratory context determined by these sensors, the system applies compressive force in the expiratory phases and releases it in the inspiratory phases. Since the system can quantify the assistance performance by comparing VFR and MAV observed in assisted states with those in unassisted states, the force level can be resiliently adjusted to maintain consistent assistance performance.

Using the abovementioned operational interface, the system is controlled in two stages: 1) the upper level involves context-aware control in which a set of gain values for the lower level force control are selected to best assist the ongoing respiratory function, and 2) the lower level involves force control of belt-driven mechanism, characterized by the gains selected by the upper-level control, to leverage VFR and MAV measurements as feedback to resiliently synchronize the assistive drive to the respiratory effort of a user. A real-time embedded controller (myRIO-1900, National Instruments) was used to implement the overall control algorithm.

On top of the proposed resilient context-aware control policy, an array of safety criteria were implemented to ensure the safety of user–system interaction by preventing overdriving (and in turn, damaging) the user. First, the maximum allowable force of the system was specified based on the review of manual assistive procedures generally given in therapy sessions while limiting the intra-abdominal pressure within a safe range [37], [38]. Second, the speed of abdominal deformation was limited within a rate of 3 cm/s to prevent sudden actuation. Third, the maximum level of MAV in both inspiration and expiration was limited to prevent hyperventilation. For participants with relatively mild disabilities, the maximum level of MAV was set to the same level as a typical healthy person. Once this state is reached, the level is decreased to 80% of the maximum, and then the system undergoes a cool-down span of 10 s for the user to recover. For participants with severe disabilities, the maximum level was even lowered to conservatively preserve safety. The assistance strategies of Exo-Abs are visually demonstrated in the supplementary videos.

III. Human–System Interaction Modeling

To design and analyze our assistive control policy, we derive a lumped-parameter model that can describe the lung dynamics subject to the abdominal cavity compression provided by Exo-Abs (Fig. 9). The model of belt-driven abdominal cavity compression was derived by combining the kinematic relation between the motor torque and the compressive force acting on the abdomen and the dynamic relation between the compressive force and abdominal cavity compression. The lung model was derived by viewing the system-driven abdominal cavity compression as supplementary respiratory effort and by introducing it to a traditional model of lung dynamics.

To facilitate our modeling, we assumed that 1) the abdominal cross-section is an ellipse, 2) the abdominal cavity has a single degree-of-freedom mechanical dynamics, and 3) the abdominal

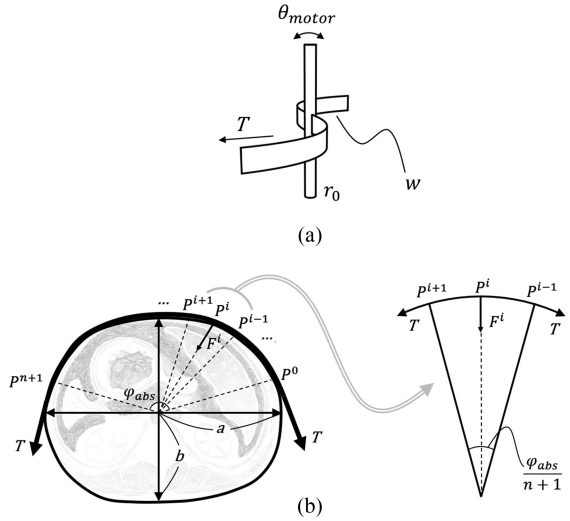

Fig. 10. Schematics for the abdominal cavity compression model. (a) Belt-wrapping mechanism for controlling tension in the actuation belt included in the proposed belt-based pressure transmission assembly. (b) Cross-section of a user's abdominal cavity and its subdivided sector, when the tension is applied by the proposed belt-based pressure transmission assembly ($x \equiv \Delta b$).

cavity is a homogeneous chamber in which pressure and volume are linear and inversely proportional to each other.

A. Exo-Abs Kinematics

Exo-Abs utilizes a single motor to control the tension in the belt-based pressure transmission assembly. By virtue of the belt assembly, the deformation of the abdominal cavity can be observed and controlled as if it has only one degree-of-freedom dynamics despite its complex geometry and compliance. The tension applied to the actuation belt is given by

$$T\ (t) = \frac{\tau_{motor}\,(t)}{r_0 + \frac{w}{\pi}\theta_{motor}\,(t)}\,. \tag{1}$$

The belt-wrapping mechanism is illustrated in Fig. 10(a). As a continuously variable transmission that changes the effective radius of the shaft depending on the rotation angle, this relation facilitates the tradeoff between effectiveness and safety by driving the robot faster when applying a relatively small force, and by driving the robot slowly when applying a relatively large force.

When the tension is applied, the force configuration around the user's abdominal cavity can be modeled as shown in Fig. 10(b). Within the area where the belt assembly is in contact with the abdominal cavity, the compressive force applied in an inward-radial direction can be expressed by

$$F^i = 2T\sin\left(\frac{\varphi_{abs}}{2\,(n+1)}\right). \tag{2}$$

Then, the net force applied to the abdominal cavity can be calculated by summing (2) along the contact area and by taking $n \to \infty$

$$\begin{aligned} F &= \lim_{n\to\infty}\sum_{i=1}^{n} F^i \\ &= \lim_{n\to\infty}\ n\cdot 2T\sin\left(\frac{\varphi_{abs}}{2\,(n+1)}\right) \\ &= \lim_{n\to\infty}\left\{\frac{2\,(n+1)}{\varphi_{abs}}\sin\left(\frac{\varphi_{abs}}{2\,(n+1)}\right)\right. \\ &\quad \left.-\frac{2}{\varphi_{abs}}\sin\left(\frac{\varphi_{abs}}{2\,(n+1)}\right)\right\}T\varphi_{abs} \\ &= T\varphi_{abs} \\ &= \frac{\varphi_{abs}}{r_0 + \frac{w}{\pi}\theta_{motor}\,(t)}\,\tau_{motor}\,(t)\,. \end{aligned} \tag{3}$$

If the belt-based pressure transmission assembly has no slack in the path, the change in the circumference of the abdominal cavity is equal to the change in the length of the actuation belt wrapped around the shaft. Therefore, the belt-based pressure transmission assembly is controlled to maintain at least a slight tension all the time for preventing slack and for faster response. Under this control approach, the amount of deformation in the abdominal cavity can be measured by the angular displacement of the motor with the relation as follows:

$$\frac{\varphi_{abs}}{2}x\,(t) = 2\int_0^{\theta_{motor}(t)}\left(r_0 + \frac{w}{\pi}\theta\right)d\theta \tag{4}$$

where the left-hand side expresses the change in the length of the belt-based pressure transmission assembly in contact with a user's abdominal cavity (by approximating the elliptic arc of the abdominal cross-section to the arc of an equivalent circle [39]), and the right-hand side expresses the change in the length of the actuation belt wrapped around the shaft of the belt-wrapping mechanism.

B. Abdominal Cavity Compression Dynamics

The dynamics associated with abdominal cavity compression can be represented by a simple mass-damper-spring system

$$m\,\ddot{x}\,(t) + c\dot{x}\,(t) + kx\ (t) = \ F\,(t)\,. \tag{5}$$

The volume change in the abdominal cavity is related to x as follows:

$$dV_{ab}\ (t) = \ \pi ah\cdot dx\,(t)\,. \tag{6}$$

Then, the pressure–volume relation in the abdominal cavity can be written by

$$\begin{aligned} P_{ab}\,(t)\,V_{ab}\,(t) \ &= (P_{ab}\,(t) + dP_{ab}\,(t)) \\ &\quad \times (V_{ab}\,(t) - dV_{ab}\,(t))\,. \end{aligned} \tag{7}$$

Since the change in the abdominal cavity volume generated by the system is small relative to its nominal volume, (7) can be

rewritten as follows:

$$dP_{ab}\ (t) = \left(\frac{V_{ab}\,(t)}{V_{ab}\,(t) - dV_{ab}\,(t)} - 1\right)\ P_{ab}\,(t)$$
$$= \frac{dV_{ab}\,(t)}{V_{ab}\,(t) - dV_{ab}\,(t)}\ P_{ab}\,(t)$$
$$\approx \frac{P_{ab}\,(t)}{V_{ab}\,(t)} dV_{ab}\,(t)\,. \tag{8}$$

C. Lung Dynamics

The pressure increase in the abdominal cavity generated by the actuation of the system can be inferred from (6) and (8). Anatomically, this pressure increase is distributed to the user's lungs and thoracic cavity, and the ratio of the distribution varies across individuals. By interpreting such a variability as a user-specific gain parameter, the effective pressure increase in the lungs due to the actuation of Exo-Abs is expressed by a heuristic gain γ as follows:

$$P^{exo}\ (t) = \ \gamma \cdot x\,(t)\,. \tag{9}$$

To represent the effect of the abdominal cavity compression on the lungs, we incorporated (9) into a simple lung dynamics model including airway resistance and lung elasticity [41]–[43] as follows:

$$R\frac{dV_{lung}}{dt} + EV_{lung} + P^{mus} + P^{exo} + \ P^{\text{PEEP}} = \ 0. \tag{10}$$

Given that Exo-Abs monitors the change in the lung volume rather than its absolute value, (10) can be rewritten to express the lung dynamics with respect to the change in the lung volume as follows:

$$R\dot{V} + EV = P^{mus} + P^{exo} \tag{11}$$

where $V_{lung} = \ -V + V^0_{lung}$, $EV^0_{lung} + \ P^{\text{PEEP}} = \ 0$, and V denotes the air usage (i.e., $\dot{V}$ and V represent VFR and MAV, respectively).

D. Model Validation With Parameter Identification Process

The overall human–system interaction model presented above is structured in a simple form. Regardless, it can cover wide-ranging use scenarios (in terms of user condition, target respiratory function, wearing configuration, and posture) by adjusting its parameters in real time. To examine the validity of the model, the model parameters are investigated while using the system.

The proposed model is comprised of state variables that can be directly measured by the system. Hence, the system can identify and update the model parameters by utilizing the data consequently accumulated during usage. Here, the least sqaures method is introduced for the identification process [43]–[48].

Theorem 1: Consider the measurement data $(\boldsymbol{H},\ \boldsymbol{y})$ with $\boldsymbol{H} \in \Re^{n\times m}$ and $\boldsymbol{y} \in \Re^n$, where m is the number of unknown parameters and n is the number of measurements. With the assumption that each element of $\boldsymbol{y}$ can be expressed with linear combination of the elements of $\boldsymbol{\theta}$, the objective function J can be defined with the measurement residual $\boldsymbol{y} - \boldsymbol{H}\hat{\boldsymbol{\theta}}$ as follows:

$$\boldsymbol{J}\ = \left(\boldsymbol{y} - \boldsymbol{H}\hat{\boldsymbol{\theta}}\right)^T\ \left(\boldsymbol{y} - \boldsymbol{H}\hat{\boldsymbol{\theta}}\right)$$
$$= \boldsymbol{y}^{\mathrm{T}}\boldsymbol{y} - \hat{\boldsymbol{\theta}}^T\boldsymbol{H}^T\boldsymbol{y} - \boldsymbol{y}^T\boldsymbol{H}\hat{\boldsymbol{\theta}} + \hat{\boldsymbol{\theta}}^T\boldsymbol{H}^T\boldsymbol{H}\hat{\boldsymbol{\theta}} \tag{12}$$

where $\hat{\boldsymbol{\theta}}$ is the estimation of $\boldsymbol{\theta}$. $\hat{\boldsymbol{\theta}}$ that minimizes $\boldsymbol{J}$ can be obtained at the extreme point of $\boldsymbol{J}$ as follows:

$$\frac{\partial \boldsymbol{J}}{\partial \hat{\boldsymbol{\theta}}} = -2\boldsymbol{y}^T\boldsymbol{H} + 2\hat{\boldsymbol{\theta}}^T\boldsymbol{H}^T\boldsymbol{H} = 0. \tag{13}$$

Solving the above equation for $\hat{\boldsymbol{\theta}}$ produces the optimal parameters to express the given data $(\boldsymbol{H},\ \boldsymbol{y})$ as follows:

$$\arg\min_{\hat{\boldsymbol{\theta}}} \boldsymbol{J} = \left(\boldsymbol{H}^T\boldsymbol{H}\right)^{-1}\boldsymbol{H}^T\boldsymbol{y}. \tag{14}$$

The solution exists if $m < n$ and $\boldsymbol{H}$ is full rank. With the sufficient data accumulation rate (1 kHz), the procedure can be frequently repeated to update the model parameters. Since the parameters are determined in a way that can optimally express the given data $(\boldsymbol{H}, \boldsymbol{y})$, the data should include full-ranged state measurements (e.g., x, $\dot{x}$, $\ddot{x}$, F, V, and $\dot{V}$) to avoid biasing of the parameters. ■

In the case of abdominal compression dynamics (5), model parameters, m, c, and k, are obtained by directly applying (14) as follows:

$$[m\ c\ k]^T = \left(\boldsymbol{H}_1^T\boldsymbol{H}_1\right)^{-1}\boldsymbol{H}_1^T\boldsymbol{y}_1 \tag{15}$$

where

$$\boldsymbol{H}_1 = \begin{bmatrix} \ddot{x}(1) & \cdots & \ddot{x}(N_1) \\ \dot{x}(1) & \cdots & \dot{x}(N_1) \\ x(1) & \cdots & x(N_1) \end{bmatrix}^T \text{ and } \boldsymbol{y}_1 = [F(1) \ldots F(N_1)]^T$$

In the case of lung dynamics (11), R and E cannot be directly obtained by applying (14) due to the unknown term P^{mus} (which is the true pressure inside the lungs). Instead, P^{mus} can be canceled out by subtracting two sets of data garnered by monitoring a user's lung dynamics with and without assistance while maintaining her/his respiratory effort in the identical level. Then, the initial estimates of R and E are obtained as follows:

$$[R\ E]^T = \left(\boldsymbol{H}_2^T\boldsymbol{H}_2\right)^{-1}\boldsymbol{H}_2^T\boldsymbol{y}_2 \tag{16}$$

where $\boldsymbol{H}_2 = \begin{bmatrix} \dot{V}_A(1) - \dot{V}_S(1) & \cdots & \dot{V}_A(N_2) - \dot{V}_S(N_2) \\ V_A(1) - V_S(1) & \cdots & V_A(N_2) - V_S(N_2) \end{bmatrix}^T$ and $\boldsymbol{y}_2 = [\gamma x(1) \ldots \gamma x(N_2)]^T$. After deriving the initial estimates of R and E, the parameters associated with the lung dynamics can be recursively updated with estimated P^{mus} which is obtained by inserting the results into (11).

In Table II, actual parameters obtained in a preliminary test with one healthy participant are shown. The standard deviations represent variations of the obtained parameter values over time in a single usage without changing the Exo-Abs installation configuration.

IV. Control Design and Analysis

We present our proposed assistive control policy and model-based analysis of user–system interaction under the proposed

TABLE II
IDENTIFIED PARAMETERS OF THE HUMAN–SYSTEM INTERACTION MODEL

	Parameter	Unit	Value
Abdominal	m	Ns^2/cm	$(3.85 \pm 0.84) \times 10^{-3}$
Compression	c	Ns/cm	$(3.27 \pm 0.45) \times 10^{-1}$
Dynamics	k	N/cm	2.84 ± 0.10
Lung	R	cmH_2Os/L	8.77 ± 1.14
Dynamics	E	cmH_2O/L	34.80 ± 0.01

Values are expressed in mean±std.
Units were expressed with original units of states for deriving the parameters (i.e., cm for x and N for F).
$1\mathrm{Ns}^2/\mathrm{cm} = 0.01$ kg and $1\ \mathrm{cmH_2O} \doteq 98.0665$ Pa.

TABLE III
PARAMETERS OF THE SYSTEM MODEL AND CONTROL POLICY

r_0	$17\ mm$	a	$19\ cm$
w	$1.6\ mm$	b	$13\ cm$
θ_0	$\pi/2\ rad$	h	$23\ cm$
k_P	$60\ N/cm$	k_R	$0.5\ cmH_2O \cdot s/L$
k_D	$180\ Ns/cm$	k_E	$5\ cmH_2O/L$

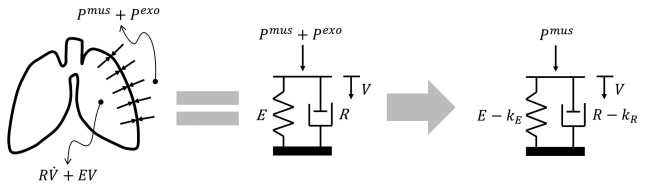

Fig. 11. Schematics for the lung dynamics model including the additional pressure generated by Exo-Abs. The resilient context-aware control reduces parameters of the lung dynamics model.

control policy. First, we show the basic form of our control policy to assist the respiratory function and analyze the closed-loop controlled lung dynamics. Second, we elaborate on our control policy for actual implementation. Third, we perform an array of simulations to validate the safety and performance of the proposed control policy.

A. Design of Resilient Context-Aware Control

Given that the overall objective of Exo-Abs is to amplify the respiratory effort, the control policy may ideally be designed with P^{mus}. However, it is practically impossible to directly measure P^{mus}. Yet, since P^{mus} leads to changes in V and $\dot{V}$, P^{exo} in (11) may instead be designed as a linear function of V and $\dot{V}$. Therefore, our proposed control policy to assist the respiratory function in a user is given by

$$P^{exo}_{ref}\ (t) = k_R\, \dot{V}\,(t) + k_E V\,(t)\,. \tag{17}$$

This control policy intends to modify the lung dynamics to ease a user's respiratory effort with reduced airway resistance and lung elasticity (Fig. 11). In this sense, our control policy is analogous to impedance control with variable stiffness [49]–[51]. Indeed, (17) reduces (11) to

$$(R - k_R)\ \dot{V} + (E - k_E)\, V\ = P^{mus} \tag{18}$$

where k_R and k_E represent decrements in R and E satisfying $0 < k_R < R$ and $0 < k_E < E$. In the Laplace domain

$$\frac{V\,(s)}{P^{mus}\,(s)} = \frac{1}{s\,(R - k_R) + (E - k_E)} \tag{19}$$

which means that, if the control policty can be realized perfectly (i.e., $P^{exo} = P^{exo}_{ref}$), 1) the steady-state volume amplification can be improved by a factor of $E/(E - k_E)$ and 2) the time constant can be improved by a factor of $E(R - k_R)/R(E - k_E)$. In this way, our control policy in (17) is resilient in that it effectively provides a user with assistive drive in accordance with their varying respiratory effort. Furthermore, it is context-aware in that the gains k_R and k_E can be adjusted to best assist the intended respiratory function (e.g., breathing, coughing, or speaking).

To achieve the intended assistance efficacy, the belt-driven pressure transmission assembly must create the motor torque τ_{motor} in (3) to elicit F that can precisely control the abdominal cavity compression dynamics in (5) to generate P^{exo} close to P^{exo}_{ref}. Given the relationship (9), the reference abdominal cavity compression x_{ref} is given by $x_{ref}\,(t) = 1/\gamma\, P^{exo}_{ref}(t)$. Hence, invoking the proportional-derivative control based on the error between x_{ref} and x

$$\tau_{motor}\,(t) = -\frac{1}{G\,(\theta_{motor})} \cdot \Big\{ k_P \left(P^{exo}\,(t) - P^{exo}_{ref}\,(t) \right) + k_D \left(\dot{P}^{exo}\,(t) - \dot{P}^{exo}_{ref}\,(t) \right) \Big\} \tag{20}$$

where $G\,(\theta_{motor}) = \frac{\varphi_{abs}}{r_0 + \frac{w}{\pi}\theta_{motor}(t)}$, the closed-loop abdominal cavity compression dynamics results

$$m\,\ddot{x}\,(t) + (c + k_D)\,\dot{x}\,(t) + (k + k_P)\,x\,(t) = k_D\,\dot{x}_{ref}\,(t) + k_P x_{ref}\,(t)\,. \tag{21}$$

Taking the Laplace transform yields the following:

$$\frac{x\,(s)}{x_{ref}\,(s)} = \frac{P^{exo}\,(s)}{P^{exo}_{ref}\,(s)}\ = \frac{k_D s + k_P}{ms^2 + (c + k_D)\,s + (k + k_P)}. \tag{22}$$

Hence, both the steady-state and transient characteristics can be shaped with k_P and k_D. Regarding the steady-state response, k_P must be selected as a large value relative to k to achieve the dc gain close to unity. Regarding the transient response, k_D must be selected as a large value to achieve overdamped response, which ensures safe user–system interaction by preventing the chattering associated with P^{exo}. If k_P and k_D are selected so that $k_D \gg k_P \gg k$, (22) approximates to a fast first-order dynamics:

$$\frac{x\,(s)}{x_{ref}\,(s)} = \frac{P^{exo}\,(s)}{P^{exo}_{ref}\,(s)}\ \approx \frac{k_D}{ms + k_D} \tag{23}$$

which implies that the desired assistive drive in (18) can be realized and that the respiratory assistance intended by our control policy can be achieved.

The nominal values of m, c , and k in (5) as well as R and E in (11) were estimated via a system identification procedure using the least squares method with data from test trials [40]. The values are summarized in Table II.

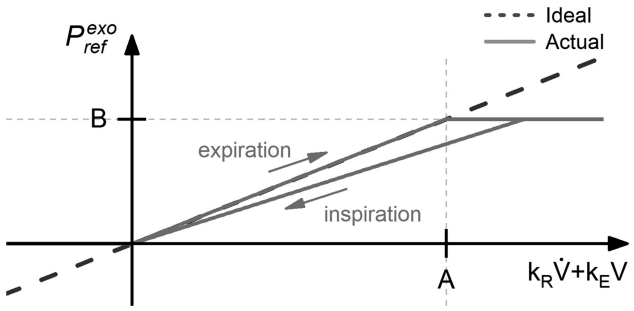

Fig. 12. Illustration of ideal P^{exo}_{ref} in (17) and actual P^{exo}_{ref} in (24). A is the condition when $\dot{V} = 2.5$ L/s and $V = 3.5$ L, and B is the condition when $x = 12$ cm. Within this nominal range, the actual control policy acts similar to the ideal control policy.

B. Implementation of Control Policy

From the previous section, we have shown that Exo-Abs can assist the user based on the proposed control policy with gain parameters properly selected for intended respiratory functions. In its actual implementation, the proposed control policy P^{exo}_{ref} is modified to embrace several criteria considering safety, user comfort, and actuation mechanism as follows:

$$P^{exo}_{ref} = \min\left(\max\left(\sigma\left(k_R^{state}\dot{V} + k_E^{state}\left(V - V^*\right)\right), \delta_0\right), P^{state}_{\max}\right). \tag{24}$$

1) State-Dependent Gain Configuration: The control policy is designed independently for each target respiratory functions (i.e., breathing, coughing, and speaking) by switching gain parameters and pressure limit depending on the superscripted variable *state*.

2) Upper-Boundedness: To ensure safety, P^{exo}_{ref} is upper-bounded with the function $\min(\cdot,\ P^{state}_{\max})$. The limiting value varies depending on the target respiratory function.

3) Lower-Boundedness: Since Exo-Abs can only transmit positive pressure to the lungs via the abdominal cavity compression, P^{exo} must be bounded to be positive. Hence, P^{exo}_{ref} is lower-bounded with the function $\max(\cdot,\ \delta_0)$, where δ_0 is a negligibly small positive pressure reference to ensure the belt assembly to maintain tension all the time.

4) Assist/Release Biasing: If P^{exo} is large when the user is inhaling, the user may feel the interaction with Exo-Abs as a resistance. Release of the pressure can be amplified with the function $\sigma = \begin{cases} 1, \dot{V} > 0 \\ \varepsilon, \dot{V} \leq 0 \end{cases}$, where ε is a small value satisfying $0 < \varepsilon < 1$ to decrease P^{exo} faster when the user is inhaling. In this way, Exo-Abs can reduce the resistive effect and can prepare for upcoming actuation in advance.

5) Phase Aligning: By assigning V^* as $V(t^*)$, where t^* is the recent time when the user is switching from inspiration to expiration (i.e., $\dot{V}(t^* - \delta) < 0$ and $\dot{V}(t^* + \delta) > 0$), Exo-Abs can align assistance with the initial point of each expiration.

Despite nonlinearity and complexity, (24) appears to function similarly to (17) in diverse scenarios as shown in Fig. 12. The performance of the implemented control policy is studied with simulations and experiments in following sections.

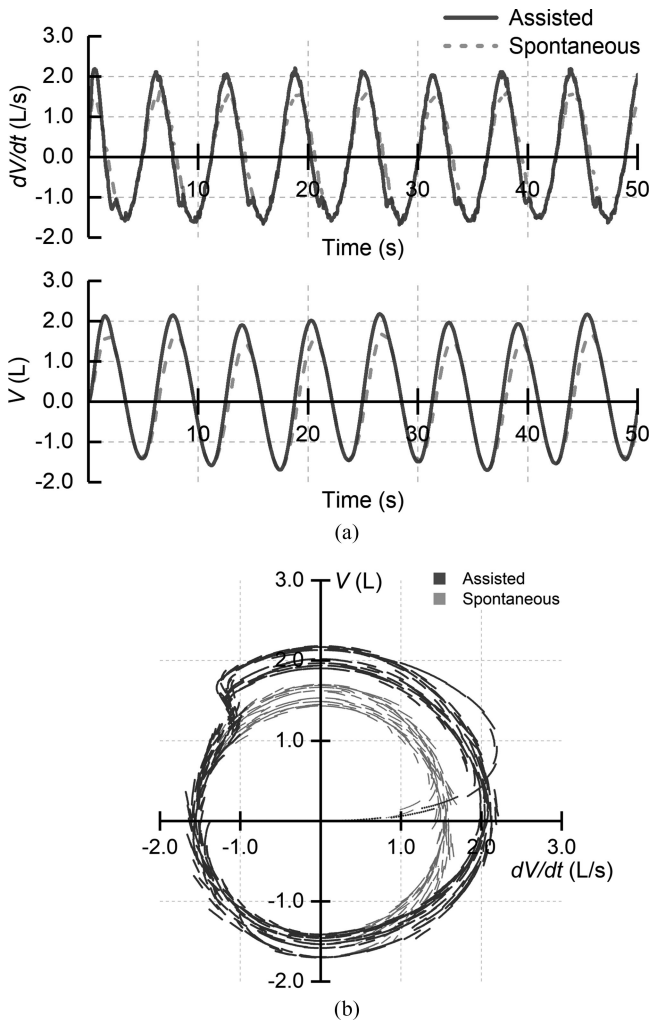

Fig. 13. Simulation results of human breathing with and without assistance. (a) $\mathrm{d}V(t)/dt$ and $V(t)$ are plotted. Note that the positive plane represents expiratory phases. (b) Limit cycles are plotted. The right-upper part of the limit cycle is expanded when assisted, without divergence.

C. Simulation of Human Breathing With and Without Exo-Abs

Before performing in-human experiments, the feasibility of Exo-Abs was evaluated in simulations. The abdominal cavity compression and lung dynamics parameters in Table III were used to simulate the breathing of a typical user. A sine function with an amplitude of 55 $\mathrm{cmH_2O}$ was used as P^{mus} [52], [53]. A white noise with a frequency of 10 Hz was added to P^{mus} as intrabreathing variability, and another white noise with a frequency of 0.3 Hz was added to P^{mus} as interbreathing variability. The same safety criteria implemented in the actual Exo-Abs was implemented precisely in the simulation. The simulation is performed in MATLAB/SIMULINK (R2019a, MathWorks).

The results of the simulation are illustrated in Fig. 13. Exo-Abs with the proposed control policy could increase VFR and MAV in the lungs during the expiratory phases. In addition, it is observed that Exo-Abs can assist a user continuously without divergence. Since the respiratory function is vital in humans, it is important for Exo-Abs to not push the users to their extreme

respiratory capacity. The limit cycle in Fig. 13(b) ascertains that Exo-Abs with the proposed control policy can maintain the user's respiratory function within physiological limits, which means that the stability of the user–system interaction may be preserved by virtue of the resiliency of the control policy and the added safety criteria.

D. Stability Analysis of Control Policy

For practicality, the control law (20) subject to (17) or (24) is designed in an intuitive form to accommodate even nonengineers such as assistants, clinicians, and therapists. Accordingly, it is advantageous to establish stability and safety critera of the control policy based on ranges of its state variables while avoiding the treatment of complex cross-state terms that may disturb the intuitiveness. In order to facilitate analysis, we adopt the *input-to-state stability* [54]–[56].

Definition 1: The system $\dot{\boldsymbol{x}} = f(\boldsymbol{x}, \boldsymbol{u})$ is *input-to-state stable* if there exist a class $\mathcal{KL}$ function β and a class $\mathcal{K}$ function α such that for any $t_0 \geq 0$, any initial state $\boldsymbol{x}(t_0)$, and any bounded input $\boldsymbol{u}(t)$, the solution $\boldsymbol{x}(t)$ exists for all $t \geq t_0$ and satisfies the following condition:

$$\|\boldsymbol{x}\| \leq \max\left\{\beta\left(\|\boldsymbol{x}\left(t_0\right)\|,\, t - t_0\right),\, \alpha\left(\sup_{t_0 \leq \tau \leq t} \|\boldsymbol{u}\left(\tau\right)\|\right)\right\}, \quad \forall t \geq t_0. \tag{25}$$

As shown in (25), the *input-to-state stability* requires the overall system to remain bounded with a bounded input. In order to reify the boundary condition, the equivalent form introduced in [57] is utilized with a Lyapunov-like function V_{ISS} as follows:

Definition 2: Suppose $f(\boldsymbol{x}, \boldsymbol{u})$ is *Lipschitz* in all $\boldsymbol{x} \in \Re^n$ and $\boldsymbol{u} \in \Re^m$. Let $V_{ISS}(\boldsymbol{x})$ be a smooth function that satisfies following inequalities for all $(\boldsymbol{x}, \boldsymbol{u})$:

$$\alpha_1\left(\|\boldsymbol{x}\|\right) \leq V_{ISS}\left(\|\boldsymbol{x}\|\right) \leq \alpha_2\left(\|\boldsymbol{x}\|\right) \tag{26}$$

$$\frac{\partial V_{ISS}}{\partial \boldsymbol{x}} f\left(\boldsymbol{x}, \boldsymbol{u}\right) \leq -W_3\left(\|\boldsymbol{x}\|\right) \text{ whenever } \boldsymbol{x} \geq \rho\left(\|\boldsymbol{u}\|\right) \tag{27}$$

where α_1 and α_2 are class $\mathcal{KL}_\infty$ functions, ρ is class $\mathcal{K}$ function, and $W_3(\boldsymbol{x})$ is a continuous positive definite function on $\Re^n$. Then, the system $\dot{\boldsymbol{x}} = f(\boldsymbol{x}, \boldsymbol{u})$ is *input-to-state stable* with $\alpha = \alpha_1^{-1} \cdot \alpha_2 \cdot \rho$, where α is a class $\mathcal{K}$ function defined in (25).

The stability criteria for Exo-Abs can be directly derived by applying the above definition to the closed-loop human–system interaction model.

Theorem 2: The overall human–system interaction with the proposed control policy (20) is *input-to-state stable*.

Proof: Let $V_{ISS}^1 = 1/2\ kx^2 + 1/2\ m\dot{x}^2$ for the abdominal compression dynamics (5) and $V_{ISS}^2 = 1/2\ RV^2$ for the lung dynamics (11). The first condition (26) can be directly satisfied with both V_{ISS}^1 and V_{ISS}^2 as follows:

$$\frac{1}{2} Z_L \left(x^2 + \dot{x}^2\right) \leq V_{ISS}^1 \leq \frac{1}{2} Z_U \left(x^2 + \dot{x}^2\right) \tag{27}$$

$$\frac{1}{2} R_L V^2 \leq V_{ISS}^2 \leq \frac{1}{2} R_U V^2 \tag{28}$$

where $Z_L \leq \min(k, m)$, $\max(k, m) \leq Z_U$, and $R_L \leq R \leq R_U$. Then, the derivatives satisfy the following inequalities:

$$\begin{aligned} \frac{d}{dt} V_{ISS}^1 &= kx \cdot \dot{x} + m\dot{x} \cdot \ddot{x} \\ &= -c\dot{x}^2 + \dot{x}F \\ &= -\left(c - \theta_1\right)\dot{x}^2 - \theta_1 \dot{x}^2 + \dot{x}F \\ &\leq -\left(c - \theta_1\right)\dot{x}^2 \ \forall \|x\| \geq \frac{\|F\|}{\theta_1} \end{aligned} \tag{29}$$

with $0 < \theta_1 < c$ and

$$\begin{aligned} \frac{d}{dt} V_{ISS}^2 &= RV \cdot \dot{V} \\ &= -EV^2 + V\left(P^{mus} + P^{exo}\right) \\ &= -\left(E - \theta_2\right)V^2 - \theta_2 V^2 + V\left(P^{mus} + P^{exo}\right) \\ &\leq -\left(E - \theta_2\right)V^2 \ \forall [V] \geq \frac{\|P^{mus} + P^{exo}\|}{\theta_2} \end{aligned} \tag{30}$$

with $0 < \theta_2 < E$. Therefore, the abdominal compression dynamics (5) with ultimate bound $x^2 + \dot{x}^2 \leq \frac{Z_U}{Z_L} \cdot \frac{\sup\|F\|}{\theta_1}$ and the lung dynamics (11) with ultimate bound $\|V\|^2 \leq R_U/R_L \cdot (\sup\|P^{mus} + P^{exo}\|)/\theta_2$ are *input-to-state stable* with bounded inputs F, P^{mus} , and P^{exo}. Since it is known that the stability condition is conserved after the cascade connection of *input-to-state stable* systems [58], [59], the overall human–system interaction is also *input-to-state stable*. ■

In addition to the stability, three noteworthy features can be derived from the above criteria. First, the subject-specific safety criteria can be obtained based on a user's measurements. For example, the ultimate bound for the lung dynamics can be set to limit air usage less than their vital capacity *VC* of the user (i.e., design P^{exo} to satisfy $\frac{\sup\|P^{mus}\| + \sup P^{exo}\|}{E} < VC$ after performing a lung function test to estimate $\sup\|P^{mus}\|$). Second, the *input-to-state stability* implies system robustness to disturbances [57]. Considering the form of the overall human–system model, there may exist error from actual nonlinear behaviror or from parameter variations (Table II). System robustness is also important in practical use scenarios since custom parameter tunings are available. Thrid, the analysis remains valid with further improvement of the model or the control policy. For example, the stability criteria (27)–(30) can be directly applied with imroved physiological modeling of P^{mus} or advanced control policy P^{exo}.

V. Experiments and Results

For preliminary proof-of-concept investigation, we designed two pilot tests and three main experiments to verify the validity of Exo-Abs and its applicability to users with insufficiency in respiratory functions. Ten research participants (mean age 34.1 ± 6.62 years, all male, Table IV) with different respiratory conditions were recruited in this article. Data were acquired in real time during each experiment to compare performance of the respiratory functions with and without the proposed robotic assistance. The analysis was performed based on the monitored

TABLE IV
INFORMATION OF THE RESEARCH PARTICIPANTS

Participant no.	Age	Gender	Condition		Participation				Note	Indication
					Pilot test	Breathing experiment	Coughing experiment	Speaking experiment		
1	28	Male	Healthy		O	-	-	-	-	Healthy participant
2	46	Male	Amyotrophic lateral sclerosis		O	-	-	-	In early stage when tested Difficulty in mastication	ALS participant
3	36	Male	Parkinson's disease		O	O	-	-	Dysarthria	PD participant
4	44	Male	Cervical spinal cord injury	C6	-	O	-	-	-	SCI participant 1
5	32	Male		C5	-	O	O	O	Choir member Speech therapy experienced	SCI participant 2
6	31	Male		C5	-	O	O	O	Choir member Speech therapy experienced	SCI participant 3
7	30	Male		C4	-	O	O	O	Under speech therapy	SCI participant 4
8	25	Male		C4	-	O	-	-	-	SCI participant 5
9	34	Male		C4	-	O	-	-	-	SCI participant 6
10	35	Male	Stroke		-	-	-	O	Dysarthria Under speech therapy	Stroke participant

34.1 $\pm$ 6.62 (years).

VFR, MAV, and voice level to analyze the dynamic respiratory states in all participants. The participants utilized their own wheelchairs or used a prepared reference wheelchair during the experiments.

All experimental procedures were conducted following approved guidelines and regulations and proceeded under the supervision of therapists. Ethical approval for the experimental protocols (B01908/561-002) was obtained from the Institutional Review Board of Seoul National University Hospital Biomedical Research Institute, Seoul, Republic of Korea. Informed consent was obtained from all the participants after explaining the possible consequences of the study.

All the data were collected with the same real-time controller (myRIO-1900, National Instruments) used to control Exo-Abs while performing experiments. VFR, MAV, chest stretch, tension applied to the actuation belt, displacement, audio signal, control parameters, and time were recorded at a rate of 1 kHz in each trial. Logged data were analyzed using MATLAB (R2019a, The MathWorks). In each participant, the comparison between two or more states was performed by the paired two-sample *t*-test. For overall comparison using datasets associated with multiple participants, the Wilcoxon rank-sum test was performed. The significance level was set as 0.05 for all the statistical tests. All statistical values were noted with the mean and standard deviation.

A. *Demonstration of Assistance Strategy via Pilot Tests*

Prior to the main experiments, two pilot tests were performed to verify the key functionality of Exo-Abs including the monitoring ability and assistance strategy. The goal of the first pilot test was to check the ability of Exo-Abs to monitor the respiratory states of users with diverse respiratory conditions, while the goal of the second pilot test was to demonstrate the feasibility of the proposed context-aware assistance strategy in real-world scenarios.

In the first pilot test, calm and spontaneous breathing of three participants including one healthy participant, one participant with amyotrophic lateral sclerosis, and one participant with Parkinson's disease was monitored by Exo-Abs (Fig. 14). Although the basic respiratory function parameters associated with normal, sclerotic, and Parkinson's disease conditions have been widely reported [19], [60], [61], they were reexamined with the sensors embedded in Exo-Abs to check if the dynamic characteristics that are difficult to capture using average values could be garnered. The results based on the spirometer showed that all average VFR and MAV of the healthy participant were larger than those of the other participants. The average VFR of the healthy participant was 21% larger than those of the two other participants ($p < 0.001$ for both inspiration and expiration), and the average MAV of the healthy participant was 194% larger than the participant with amyotrophic lateral sclerosis and 204% larger than the participant with Parkinson's disease ($p < 0.001$ for both inspiration and expiration). Detailed results are presented in Table V. Through this pilot test, we verified that Exo-Abs could monitor the respiratory states of patients associated with various respiratory functions. We also observed that the shape of each VFR pulse demonstrated unique patterns for each participant. To enable the switching between spirometer feedback and chest-belt plethysmograph feedback during real-time respiratory assist, two VFR signals were simultaneously measured with both the spirometer and the plethysmograph on an individual basis, which were used to construct a simple calibration relationship between the two VFR signals. In this way, Exo-Abs can provide personalized and physiological assistance based on both sensors.

In the second pilot test, the performance of breathing assistance was evaluated with one healthy participant to check the

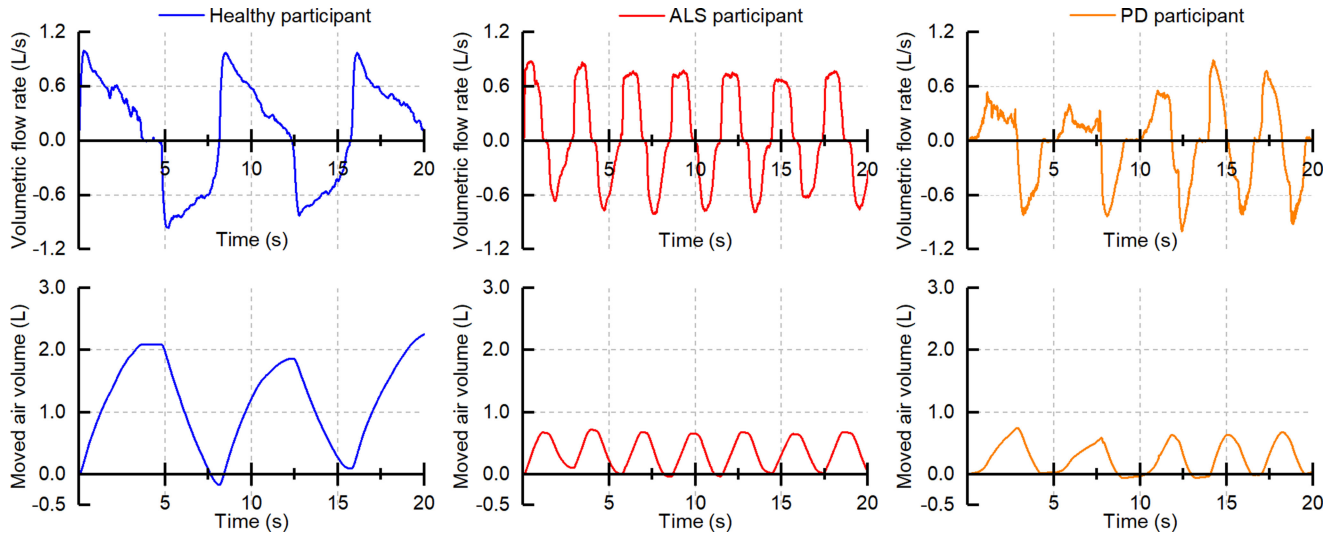

Fig. 14. Baseline measurements of a healthy participant, a participant with amyotrophic lateral sclerosis, and a participant with Parkinson's disease to check the functionality of the sensors. Subtle differences in breathing patterns were captured. The healthy participant showed larger VFR and MAV compared with the other participants ($p < 0.001$ in all cases), with slower respiratory rates ($p < 0.001$ for both cases).

TABLE V
DETAILED INFORMATION FOR THE PILOT TESTS

Pilot test 1: Baseline measurements for validating sensors

Participant	f (breaths /min)	$\overline{VFR_e}$ (L/sec)	$\overline{VFR_i}$ (L/sec)	$\overline{MAV_e}$ (L)	$\overline{MAV_i}$ (L)
Healthy participant	7.43±0.01	0.94±0.10	0.91±0.07	1.99±0.40	1.93±0.35
ALS participant	20.54±0.02	0.79±0.07	0.74±0.07	0.67±0.03	0.67±0.05
PD participant	16.73±0.08	0.69±0.17	0.86±0.05	0.64±0.10	0.65±0.07

Pilot test 2: Validation of the assistance algorithm

State	f (breaths /min)	$\overline{VFR_e}$ (L/sec)	$\overline{VFR_i}$ (L/sec)	$\overline{MAV_e}$ (L)	$\overline{MAV_i}$ (L)
Unassisted	25.38±0.06	1.35±0.13	1.37±0.11	1.01±0.23	1.19±0.06
Assisted (precise)	23.68±0.04	1.95±0.08	1.82±0.12	1.54±0.07	1.92±0.30
Assisted (casual)	23.66±0.05	1.79±0.09	1.65±0.12	1.52±0.07	1.84±0.31

The healthy participant showed greater values than the others ($p < 0.001$) in every parameter. Respiratory parameters of patients with weakened respiratory ability could be measured with high sensitivity.
Values are expressed in mean±std.
Values from the unassisted state of the healthy participant showed smaller values than the others ($p < 0.001$) except for the respiratory rate. Both the assisted states showed no significant difference.
Values are expressed in mean±std.

validity of the proposed resilient context-aware control scheme (Fig. 15). The test was repeated using 1) the spirometer and 2) the chest-belt plethysmograph as feedback to compare the performance of Exo-Abs when operating with these alternative sensors. After 3 min of spontaneous breathing, the participant was asked to use Exo-Abs. The participant was asked to maintain a constant respiratory rate of 25 breaths/min by listening to a metronome. The assistance level was set to a maximum force of 70 N. The force was applied in synchronization with and proportion to each expiration measured by the employed feedback sensor. When the participant received assistance by Exo-Abs based on the spirometer (noted as "precise feedback"), the average expiratory VFR increased by 44% ($p < 0.001$) from 1.35 ± 0.13 to 1.95 ± 0.08 L/s, and the average expiratory MAV increased by 52% ($p < 0.001$) from 1.01 ± 0.23 to 1.54 ± 0.08 L. In addition, improvements were also observed in the inspiratory parameters. The average inspiratory VFR increased by 33% ($p < 0.001$) from 1.37 ± 0.11 to 1.82 ± 0.12 L/s, and the average inspiratory MAV increased by 61% from 1.19 ± 0.06 to 1.92 ± 0.30 L. Similarly, when the participant received assistance based on the chest-belt plethysmograph (noted as "casual feedback"), the average expiratory/inspiratory VFR increased by 33% and 20% to 1.79 ± 0.09 and 1.65 ± 0.12 L/s, respectively ($P < 0.001$), and the average expiratory/inspiratory MAV increased by 51% and 55% to 1.52 ± 0.07 and 1.84 ± 0.31 L, respectively ($p < 0.001$). In addition, the degree of improvements in VFR and MAV was not significantly different between Exo-Abs operated with the precise feedback and the casual feedback ($p \geq 0.05$). In summary, the pilot test showed the validity of Exo-Abs in assisting both expiratory and inspiratory phases of the breathing function. Detailed statistical parameters are shown in Table V.

B. Assistance Performance for Breathing

As a fundamental respiratory function, the assistance performance for breathing was studied by applying breath-by-breath assistance to actual target users. One participant with Parkinson's disease (Fig. 16) and six participants with cervical spinal cord injuries were tested. Participants were requested to forcefully breathe during both the unassisted and assisted states while naturally adjusting their respiratory rates to avoid hyperventilation. For each participant, a comparison between the unassisted and assisted states was performed to examine the statistical differences caused by the assistance. The maximum force level of 90 N was met, which was recommended by the

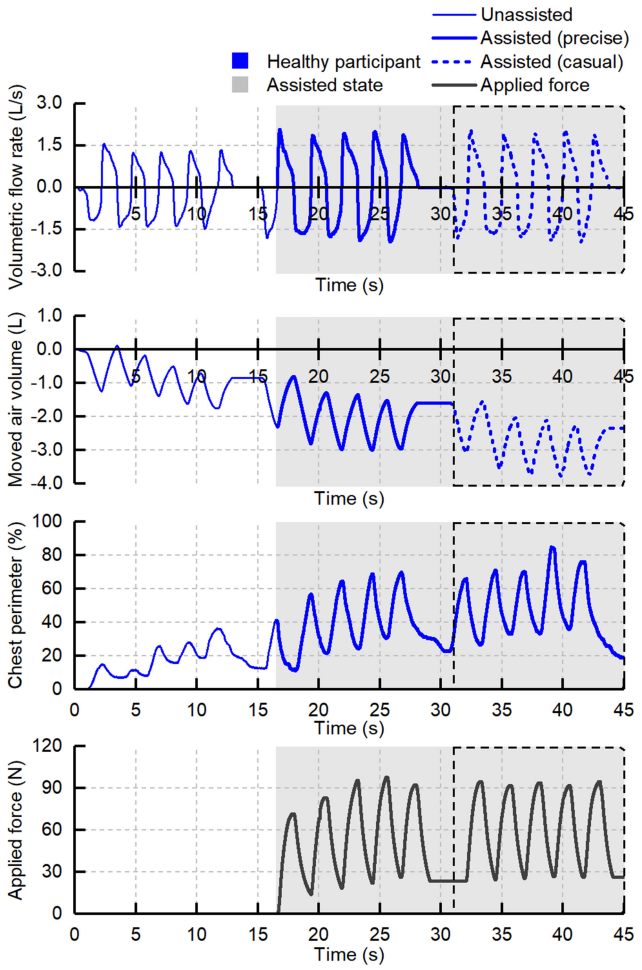

Fig. 15. Demonstration of the assistance algorithm in the second pilot test. Increased VFR and MAV were seen in the assisted state compared to unassisted state (white area, $p < 0.001$ in all cases), both with precise feedback (spirometry and plethysmography, grey-backgrounded) and with casual feedback (plethysmography-only, dash-boxed). No significant differences were observed between the precisely assisted state and casually assisted states. Respiratory rates in all states remained at the same level ($p < 0.05$). After several actuations, the system identifies the region responsible for a user's clothing and cancels it out.

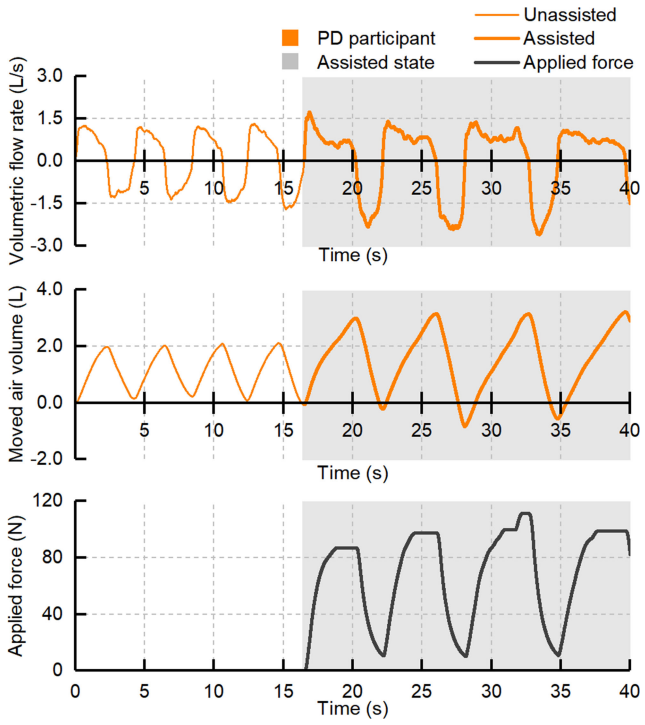

Fig. 16. Demonstration of the breathing assistance process. In the assisted state (grey-background), a maximum 120 N of force was applied in synchronization with the expiratory VFR (positive: expiration and negative: inspiration).

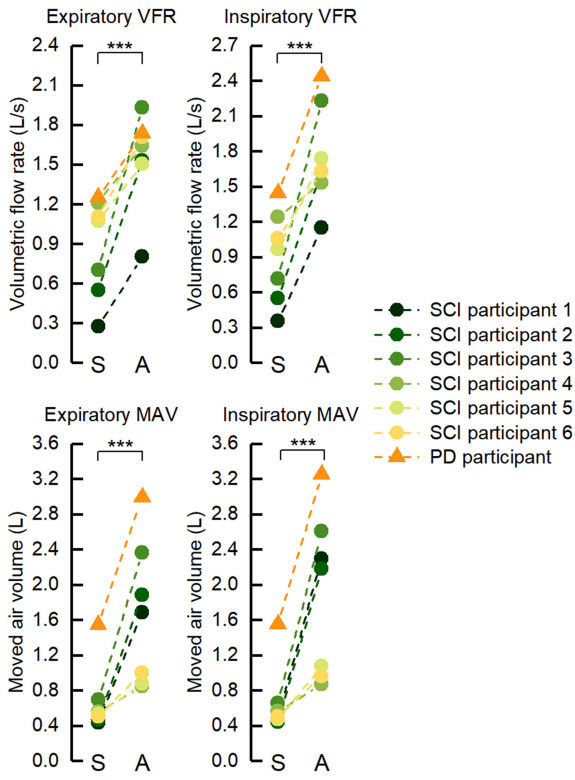

Fig. 17. Overall results of the breathing experiment. "S" stands for spontaneous breathing (unassisted state) and "A" stands for assisted breathing (assisted state). Expiratory VFR, inspiratory VFR, expiratory MAV, and inspiratory MAV showed significant increases in the assisted state, compared to the unassisted state, in each participant. $^{***}p < 0.001$.

observing medical staff. In this level of assistance, participants were able to continue to breathe with assistance for more than 15 min without discomfort. Before collecting experimental data, each participant had sessions of freely using Exo-Abs to adapt to how it operated.

The results showed that the assistance significantly amplified both expiratory and inspiratory parameters in each participant (Fig. 17). On the average, expiratory VFR increased by 0.67 ± 0.31 L/s ($p = 0.0013$); expiratory MAV increased by 0.99 ± 0.59 L ($p = 0.0044$); inspiratory VFR increased by 0.85 ± 0.39 L/s ($p = 0.0011$); and inspiratory MAV increased by 1.22 ± 0.73 L ($p = 0.0043$). When compared to the unassisted state, average improvements of 101.43%, 121.95%, 162.09%, and 201.96% were observed, respectively. In every trial for each participant, the changes were significant at the level of $p < 0.001$ (Table VI).

TABLE VI
DETAILED INFORMATION FOR THE EXPERIMENT ON ASSISTANCE PERFORMANCE FOR BREATHING

Participant	State	$\overline{VFR_e}$ (L/sec)	$\overline{VFR_i}$ (L/sec)	$\overline{MAV_e}$ (L)	$\overline{MAV_i}$ (L)
SCI participant 1	unassisted	0.28±0.06	0.36±0.04	0.44±0.09	0.51±0.09
	assisted	0.81±0.41	1.15±0.39	1.69±0.66	2.30±0.57
SCI participant 2	unassisted	0.55±0.07	0.55±0.06	0.47±0.08	0.45±0.05
	assisted	1.53±0.11	1.63±0.18	1.89±0.20	2.18±0.40
SCI participant 3	unassisted	0.71±0.04	0.72±0.08	0.70±0.10	0.66±0.05
	assisted	1.94±0.18	2.23±0.25	2.37±0.24	2.61±0.35
SCI participant 4	unassisted	1.22±0.15	1.24±0.09	0.56±0.11	0.57±0.06
	assisted	1.64±0.08	1.53±0.08	0.85±0.09	0.87±0.07
SCI participant 5	unassisted	1.07±0.22	0.97±0.25	0.54±0.14	0.48±0.13
	assisted	1.51±0.14	1.74±0.10	0.88±0.08	1.08±0.11
SCI participant 6	unassisted	1.11±0.20	1.06±0.07	0.51±0.09	0.51±0.05
	assisted	1.71±0.19	1.63±0.28	1.00±0.12	0.97±0.24
PD participant	unassisted	1.57±0.06	1.81±0.23	2.42±0.10	2.44±0.21
	assisted	1.74±0.26	2.44±0.14	3.75±0.78	4.07±0.29

In every participant, the assisted cases showed greater values compared to the unassisted cases ($p < 0.001$).
Values are expressed in mean ±std.

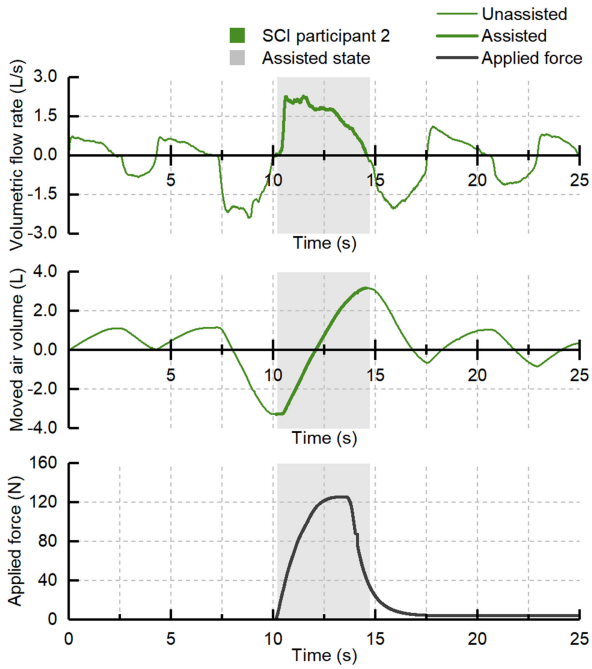

Fig. 18. Demonstration of the coughing assistance process. In the assisted state (grey-backgrounded), a maximum 150 N of force was applied in synchronization with the expiratory VFR, only after detecting a large MAV (positive: expiration and negative: inspiration).

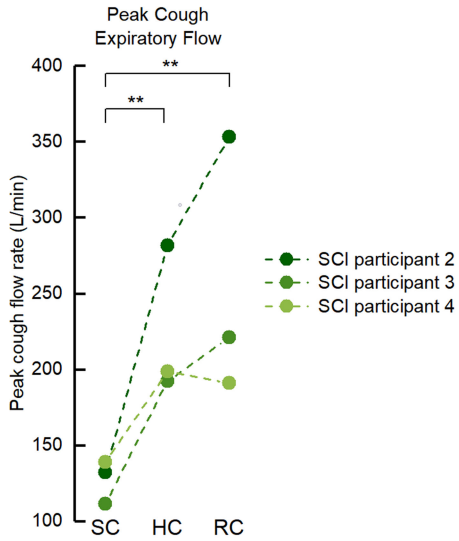

Fig. 19. Overall results of the coughing experiment. "SC," "HC," and "RC" stand for spontaneous cough (unassisted state), human-assisted-cough (assisted with a user's own alternative method of support; self-assist or medical-staff-assist), and robot-assisted-cough (assisted state), respectively. For both HC and RC, significant increases in PCEF were measured, while showing no significant difference between the two cases for each participant. $^{**}p < 0.01$.

C. *Assistance Performance for Coughing*

A successful cough, a process of removing mucus from the airway, requires a large amount of air to move out of the body at a high flow rate. This demands highly dynamic mechanical responses from Exo-Abs. In this experiment, three types of cough were compared to examine the effectiveness of the assistance to the participants and the availability of Exo-Abs to provide such assistance. The three types of cough included a spontaneous cough (SC), human-assisted cough (HC; including both self-assistance and medical-staff-assistance), and robot-assisted cough (RC). Three participants with cervical spinal cord injuries (noted as SCI participants 2 to 4) were tested. Each participant had experiences of sporadic failure in SC, and they had their own approaches to support coughing. One participant could bend over in synchronization as personal support for coughing for the HC (SCI participant 2, also known as "self-assisted cough"), while the other participants required assistance from medical staff to apply force on their abdomen for the HC (SCI participants 3 and 4, also known as "manually assisted cough") [62], [63]. In each case, participants were asked to try cough when they were ready, while performing spontaneous breathing to gain the momentum to cough. Repetition was performed with a break of more than 1 min to avoid overstraining of their lungs. After free trials wearing the system, the maximum force level of 150 N was met, which was recommended by medical staff and was similar to the level of assistance given by companions. The force was applied following the expiratory VFR, where its initiations were made only after a large amount of inhalation was detected (Fig. 18). The measurements were observed similarly to the breathing assistance experiments, while the peak cough expiratory flow (PCEF) was collected as an index for coughing ability in this case.

Both the HC and RC showed a significant increase in PCEF values, compared to the SC (Fig. 19). With the average baseline PCEF of 127.75 L/min in the SC, an increased PCEF of 224.40 L/min in the HC ($p = 0.0024$), and 255.11 L/min in the RC ($p = 0.0093$) were observed. In addition, considering that the PCEF of 160 L/min is used as a medical criterion

TABLE VII
DETAILED INFORMATION FOR THE EXPERIMENT ON ASSISTANCE PERFORMANCE FOR COUGHING

Participant	State	PCEF (L/min)	SC<HC	SC<RC	HC<RC
SCI participant 2	SC	132.43±40.12	P<0.001	P<0.001	P=0.0338
	HC	281.77±90.22			
	RC	353.14±34.96			
SCI participant 3	SC	111.63±5.91	P<0.001	P<0.001	P=0.2302
	HC	192.50±39.64			
	RC	221.19±60.85			
SCI participant 4	SC	139.20±36.99	P<0.001	P<0.001	P=0.7343
	HC	198.92±60.27			
	RC	191.01±40.14			

Values are expressed in mean±std.

for determining whether a person requires mechanically assisted coughing or not [64], the clear improvement from the PCEF below 160 L/min in the SC ($p < 0.001$) to the PCEF above 160 L/min in the HC and RC ($p < 0.001$) was observed in each participant. Detailed statistical values are included in Table VII.

D. Assistance Performance for Speaking

Human speech involves a complex process. It is highly dependent on the ability to control the vocal cord, laryngeal area, and facial muscles. However, it is also known that the ability to generate a large airflow is strongly related to the performance of speaking [1], [2]. In this experiment, the effect of assistance on speaking was studied as an extension of respiratory function by comparing recorded voice samples for 5 min in both unassisted and assisted states. Four participants included one who had experienced a stroke and three with cervical spinal cord injuries, who had also participated in the breathing and coughing experiments. These four participants had previous experiences of attending speech therapy in clinics. The assistance was given in synchronization with several words, considering a burst of words as one expiratory action (Fig. 20). Similar to the cough assistance, the maximum force level was set at 160 N with sufficient breaks between each trials for the patients to recover. To analyze vocal loudness, an interval in the data containing both the unassisted and assisted states was obtained. Then, regions that contained speech were extracted separately to produce data samples for comparison. The difference between the samples was expressed in decibels, i.e., the sound pressure of each state was obtained by the root-mean-square of the sound pressures over time.

Under an identical recording environment, participants showed an average improvement in vocal loudness of 8.3615 dB while assisted ($p < 0.001$) compared to their unassisted speech (Fig. 21). In addition to the vocal loudness, it was noted that other vocal parameters such as speech clarity or maximum pitch were also improved. Particularly, the participant who had experienced a stroke, who was also diagnosed with dysarthria, could deliver clearer words. The results are further explored in the Discussion section.

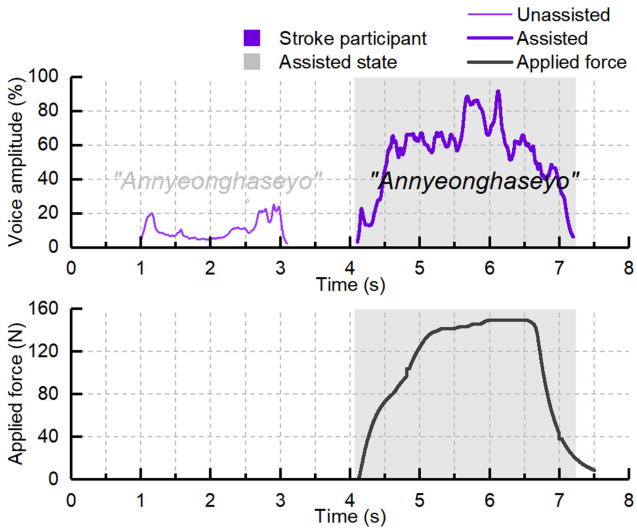

Fig. 20. Demonstration of the speaking assistance process for the spoken phrase *Annyeonghaseyo*. In the assisted state (grey-background), a maximum 160 N of force was applied in synchronization with the audio signal from the microphone, interpreting it as an expiratory motion.

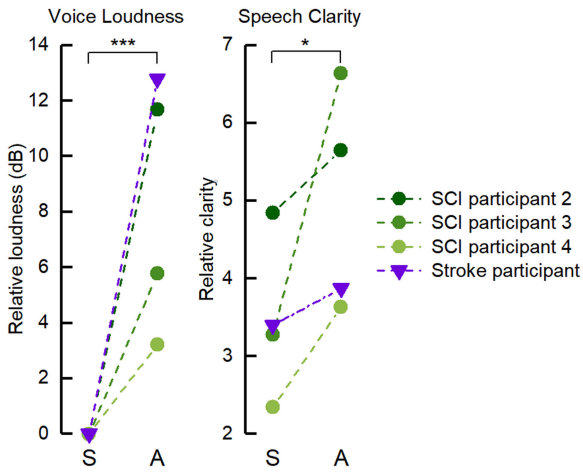

Fig. 21. Overall results of the speaking experiment. "S" stands for spontaneous speaking (unassisted state) and "A" stands for assisted speaking (assisted state). The average voice loudness showed a significant increase in the assisted state compared to the unassisted state in all the participants. $^{***}p < 0.001$. The average speech clarity showed a significant increase in the assisted state, compared to the unassisted state, in all the participants. $^{*}p = 0.0101$.

E. Survey Study for Assessing Assistance Performance in Speech Clarity

During the speaking experiment, the voice loudness of the recordings was measured and analyzed to evaluate the effectiveness of assistance by Exo-Abs. However, especially in the case of the participant after stroke, we observed that the participant not only could make louder voice, but also could speak out words more clearly. To inspect this phenomenon further, we performed a survey study with nine voice samples of the participant extracted from recordings during the speaking experiment. Twenty participants were recruited as evaluators. The voice samples are included in the supplementary data files. To assess speech clarity, MIRtoolbox was used [66]. The toolbox had a built-in pulse

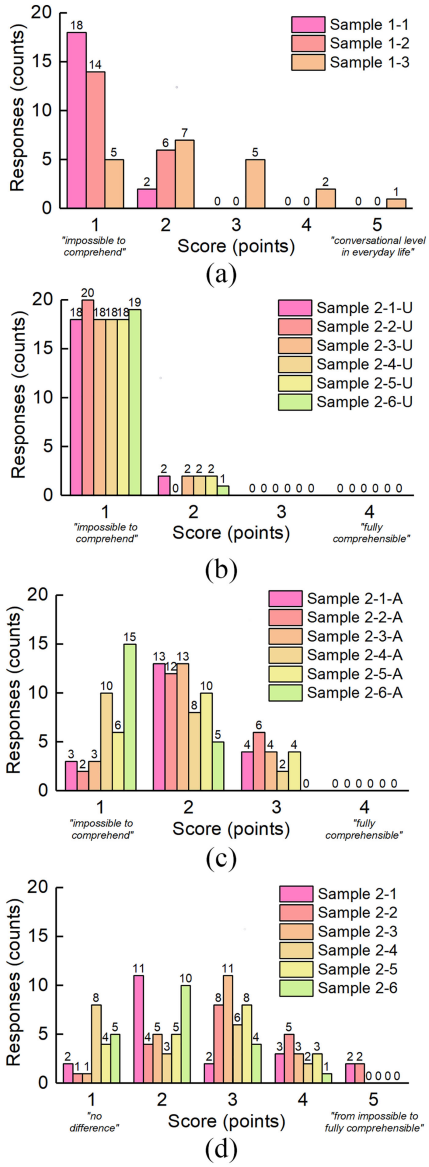

Fig. 22. Results of the survey to investigate assistance performance for speech clarity. (a) Baseline inquiries on the comprehensibility of speech samples. (b) Comprehensibility tests on samples extracted from the unassisted state. (c) Comprehensibility tests on samples extracted from the assisted state. (d) Subjective assessments of the increase in comprehensibility.

clarity function that can assess the pulse clarity of a given sound sample. Visualization and offline analysis were performed via Praat [67].

First, three voice samples under the unassisted state (noted as "Sample 1-1" to "Sample 1-3") were used to evaluate baseline ability to generate a clear phonation. Each evaluator was inquired to guess the word spoken out and to answer scores for the samples, from score level 1 for "impossible to comprehend" to score level 5 for "conversational level in everyday life" as in Fig. 22(a). No evaluators could correctly guess the word in "Sample 1-1." One evaluator answered correctly in the "Sample 1-2," and five evaluators answered correctly in the "Sample 1-3." For "Sample 1-1" and "Sample 1-2," there was no higher score than level 3, and most of the scores remained in level 1. For "Sample 1-3," level 2 was the most answered score by showing seven responses, and eight responses showed scores higher than level 2.

Second, the other six speech samples were used to compare the phonation clarity between the assisted state and unassisted state (noted as "Sample 2-1" to "Sample 2-6"). Each sample includes two speaking trials. One was recorded without the assistance (noted as "Sample 2-N-U"), and the other was recorded with the assistance (noted as "Sample 2-N-A"). Similarly, comprehensibility of each speaking trial was asked in scale of 1 to 4, from score level 1 for "impossible to comprehend" to score level 4 for "fully comprehensible" as in Fig. 22(b) and (c). For the trials of the unassisted state, most of the responses were scored in level 1 (above 17 responses each). Less than 10% of the evaluators responded level 2. However, for the trials of the assisted state, 20% of the evaluators responded level 3, and 51% of the evaluators responded level 2, which was encouraging. Additionally, relative increases in subjective comprehensibility for each sample were inquired, from score level 1 for "no difference" to score level 5 for "from impossible to fully comprehensible" as in Fig. 22(d). In this questionnaire, most of the responses were distributed in level 2 to level 3, whereas the sample with a complex word (Sample 2-6) showed most of the scores located in level 2.

The participant was not able to speak out words clearly due to the dysarthria from the stroke, which involves disability in their bulbar muscles. With an enhanced momentum achieved by assisting participant's expiratory effort, the participant could focus more on controlling the muscles above the neck. Through this survey study, we observed that some simple words could be assisted by Exo-Abs, thus allowing the users to have conversation with their close acquaintances, although it was still difficult to assist these people to speak out complex words.

VI. Discussion

There is an expression, "as easy as breathing." However, the simple task of breathing is not easy for some people, such as those with neurological disorders. The proposed soft wearable robotic system was designed to provide these neurological patients with resilient and context-aware assistance in prolonged therapy procedures by utilizing a mechanism that applies assistive pressure to the user's abdomen. Although the idea of applying pressure to the abdominal cavity to assist weakened respiration is not a completely new approach [5], [9], [13], existing devices have limitations in their efficacy and usability due to discomfort from the mechanism of assistance and asynchrony with the native respiratory effort. Recently, reported robotic-assistive technologies hint toward the design of a system that can enable everyday assistance by capitalizing on the recent advances in bioinspiration, soft materials, and intelligent assistance strategies. We designed a physiological and safe actuation mechanism with reference to human abdominal muscles, which natively engages in the control of the volumetric states in the lungs [22], [29]. In addition, we developed a customized sensor combination that can be used in conjunction with our actuation mechanism to realize a resilient

context-aware control policy capable of all-day assistance, inspired by the control schemes of human-assistive robots [30], [31].

The primary results of this article clearly suggest that synchronization to the user effort is the key to successful respiratory assistance. Synchronization includes not only the instantaneous alignment of the actuation with human respiratory effort but also a process of resiliently adjusting the magnitude and strategy of assistance in accordance with the respiratory context. Through this synchronization, Exo-Abs could provide bidirectional assistance during both inspiratory and expiratory phases of breathing, maximally utilizing the body recoil for inspiration through the phase-sensitive assistance. In this way, Exo-Abs could assist with functions that cannot be provided by existing mechanical ventilators.

Here, we elaborate on a few noteworthy findings garnered from our proof-of-concept experiments. First, the "resiliency" of the proposed control policy enabled Exo-Abs to respond to the participants' varying breathing patterns without individually customizing the control parameters or profiles. For example, in the breathing experiment, both PD participant and SCI participants 1–3 showed square-wave-like VFR patterns while utilizing Exo-Abs, since they preferred increasing the average amount of air moving in and out to maximizing peak inspiratory or expiratory VFR. Meanwhile, the SCI participants 4–6 showed triangular-wave-like VFR patterns by simply amplifying their unassisted VFR patterns for their comfort. However, they regulated their respiratory rates to maintain an average level of MAV in the level that they can expect. Such differences are difficult to predict in advance and highly depend on the personal preferences of users. With the resilient control policy, the process of tailoring Exo-Abs to each user with diverse respiratory characteristics can be minimized. In addition, participants could learn how Exo-Abs works easily and could guide Exo-Abs to assist in a way that they preferred.

Second, the "context-awareness" of the proposed control scheme allowed Exo-Abs to generate a synergistic assistive effect across diverse respiratory functions. In the coughing experiment, the participants could exceed the nominal performance in HC and RC if there was assistance in the free-breathing phase. They could inhale larger amounts of air with the enhanced build-up procedure, which resulted in increased PCEF values after dexterously shifting the assist strategy. In the actual experiment, there was no assistance given in this phase to Exo-Abs to distinguish enhanced inhalation from the intention to cough. The results of SCI participant 2 showed the best assistive effect in the RC case ($p = 0.0338$), while the results of SCI participants 3 and 4 showed similar assistive effects between HC and RC as in Table VII ($p = 0.2302$ and $p = 0.7303$). Considering that it was extremely challenging for the SCI participant 2 to self-synchronize to own coughs due to the reduced body mobility, Exo-Abs could result in a significant improvement in RC relative to HC. In the case of the SCI participants 3 and 4, the RC was still comparable to HC without significant difference.

Last, Exo-Abs could assist the participants with more complex respiratory functions by providing assistance to the user so as to exploit it as a "preview" to prepare for the forthcoming respiratory actions. In fact, in the speaking experiment, we observed two notable results other than the increase in vocal loudness. In the cases of SCI participants 2 and 3, the system was able to widen the vocal range of the users. As SCI participants 2 and 3 were choir members in their local churches, they demonstrated singing during the speaking experiments. While freely using Exo-Abs, they could sing the songs that they could not without assistance. Demonstration of the singing trial is included in the supplementary videos. Furthermore, the stroke participant, who also had been diagnosed with dysarthria, could deliver words more comprehensibly with the assistance. For quantitative analysis, speech intelligibility [65] is the most commonly used metric. Yet, as it requires further analysis regarding language, spatial control, or audibility (which are not the main focus of this article), we simply analyzed the recorded voice samples using pulse clarity [66] as a metric to show how the sound was distinguishable by observing the peaks of dominant frequencies in the participants' voices. The participants in the experiment showed a 42.72% improvement in pulse clarity ($p = 0.0101$) with the assistance. In addition, a survey study was performed to evaluate how effective the assistance was in the stroke patient's speaking. The results showed that the degree of improvement was sufficient to enable the participant to deliver a few comprehensible words with repetitions, although the assistance could not return the speech of the participant to the fully communication-available level.

We also acknowledge two main limitations of the article. First, the effects of the assistance were studied with heuristically set force levels. Due to the difference in mechanism between existing mechanical ventilation and Exo-Abs, the existing medical criteria for setting the target of the assistance could not be directly applied to Exo-Abs. Instead, the level of the assistance was set conservatively within the recommended level by the observing medical staff. In this way, the functionality of Exo-Abs could only be evaluated in a range except for those with severe respiratory failure. Second, further experiments with extended usage time are required. As the system is the first realization to validate the proposed interaction, the experiments could not be maintained for hours. In addition, the long-term effects with repeated uses should be studied, engaging more participants to strengthen the reliability of Exo-Abs toward patients with diverse respiratory characteristics.

In future article, we will perform further studies on the physiology and biomechanics of the respiratory system through the abdominal cavity compression, using Exo-Abs as a tool to observe interactive effects while including patients with more various physiological characteristics (i.e., age, gender, and other types of diseases). As Exo-Abs is programmed with a reactive assistance algorithm, it is used to amplify native respiratory motions. With improved understanding, we may improve Exo-Abs to precede instant respiratory motions based on a strict model to teach specific respiration methods or to train respiratory maneuvers (https://www.ems.gov/education.html). As it can help to improve safety criteria, we will also perform studies on synergistic assistive effects that can be achieved by combining Exo-Abs with existing mechanical ventilators.

REFERENCES

[1] C. Roussos, "Function and fatigue of respiratory muscles," *Chest*, vol. 88, pp. 124S–132S, 1985, doi: 10.1378/chest.88.2_Supplement.124S.

[2] A. D. Miller, A. L. Bianchi, and B. P. Bishop, *Neural Control of the Respiratory Muscles*. Boca Raton, FL, USA: CRC Press, 2019.

[3] B. M. Haas, M. Trew, and P. C. Castle, "Effects of respiratory muscle weakness on daily living function, quality of life, activity levels, and exercise capacity in mild to moderate parkinson's disease," *Amer. J. Phys. Med. Rehabil.*, vol. 83, no. 8, pp. 601–607, 2004.

[4] C. Perrin, J. N. Unterborn, C. D. Ambrosio, and N. S. Hill, "Pulmonary complications of chronic neuromuscular diseases and their management," *Muscle Nerve*, vol. 29, no. 1, pp. 5–27, Jan. 2004, doi: 10.1002/mus.10487.

[5] N. Ambrosino, N. Carpenè, and M. Gherardi, "Chronic respiratory care for neuromuscular diseases in adults," *Eur. Respir. J.*, vol. 34, no. 2, pp. 444–451, Aug. 2009, doi: 10.1183/09031936.00182208.

[6] S. Nava, P. Navalesi, and G. Conti, "Time of non-invasive ventilation," *Intensive Care Med.*, vol. 32, no. 3, pp. 361–370, Mar. 2006, doi: 10.1007/s00134-005-0050-0.

[7] A. Baydur *et al.*, "Long term non-invasive ventilation in the community for patients with musculoskeletal disorders: 46 year experience and review," *Thorax*, vol. 55, no. 1, pp. 4–11, 2000.

[8] J. O. Benditt, "Full-time noninvasive ventilation: Possible and desirable," *Respir. Care*, vol. 51, no. 9, pp. 1005–1015, 2006.

[9] S. Metha and N. S. Hill, "Noninvasive ventilation," *Amer. J. Respir. Crit. Care Med.*, vol. 163, no. 2, pp. 540–577, Feb. 2001, doi: 10.1164/ajrccm.163.2.9906116.

[10] B. Schönhofer and S. Sortor-Leger, "Equipment needs for noninvasive mechanical ventilation," *Eur. Respir. J.*, vol. 20, no. 4, Oct. 2002, Art. no. 1029, doi: 10.1183/09031936.02.00404202.

[11] I. Bergbom-Engberg and H. Haljamäe, "Assessment of patients' experience of discomforts during respirator therapy," *Crit. Care Med.*, vol. 17, no. 10, pp. 1068–1072, Oct. 1989, doi: 10.1097/00003246-198910000-00021.

[12] D. Chiumello *et al.*, "Noninvasive positive pressure ventilation delivered by helmet vs. standard face mask," *Intensive Care Med.*, vol. 29, no. 10, pp. 1671–1679, Oct. 2003, doi: 10.1007/s00134-003-1825-9.

[13] L. S. Aboussouan, "Respiratory disorders in neurologic diseases," *Cleveland Clinic J. Med.*, vol. 72, no. 6, pp. 511–520, 2005, doi: 10.3949/ccjm.72.6.511.

[14] J. Hull *et al.*, "British thoracic society guideline for respiratory management of children with neuromuscular weakness," *Thorax*, vol. 67, pp. i1–40, Jul. 2012, doi: 10.1136/thoraxjnl-2012-201964.

[15] J. Kim *et al.*, "Reducing the metabolic rate of walking and running with a versatile, portable exosuit," *Science*, vol. 365, no. 6454, pp. 668–672, Aug. 2019, doi: 10.1126/science.aav7536.

[16] L. N. Awad *et al.*, "A soft robotic exosuit improves walking in patients after stroke," *Sci. Transl. Med.*, vol. 9, no. 400, Jul. 2017, Art. no. eaai9084, doi: 10.1126/scitranslmed.aai9084.

[17] H. In, B. B. Kang, M. Sin, and K. Cho, "Exo-Glove: A wearable robot for the hand with a soft tendon routing system," *IEEE Robot. Automat. Mag.*, vol. 22, no. 1, pp. 97–105, Mar. 2015, doi: 10.1109/MRA.2014.2362863.

[18] B. B. Kang, H. Choi, H. Lee, and K.-J. Cho, "Exo-Glove poly II: A polymer-based soft wearable robot for the hand with a tendon-driven actuation system," *Soft Robot.*, vol. 6, no. 2, pp. 214–227, Dec. 2018, doi: 10.1089/soro.2018.0006.

[19] J. B. West, *Respiratory Physiology: The Essentials*. Philadelphia, PA, USA: Wolters Kluwer Health/Lippincott Williams & Wilkins, 2012.

[20] J. González-Vargas, J. Ibáñez, J. L. Contreras-Vidal, H. van der Kooij, and J. L. Pons, Eds., "Wearable robotics: Challenges and trends," in *Proc. 2nd Int. Symp. Wearable Robot.*, 2016, pp. 33–62.

[21] A. T. Asbeck, S. M. M. De Rossi, I. Galiana, Y. Ding, and C. J. Walsh, "Stronger, smarter, softer: Next-generation wearable robots," *IEEE Robot. Automat. Mag.*, vol. 21, no. 4, pp. 22–33, Dec. 2014, doi: 10.1109/MRA.2014.2360283.

[22] A. De Troyer, M. Estenne, V. Ninane, D. Van Gansbeke, and M. Gorini, "Transversus abdominis muscle function in humans," *J. Appl. Physiol.*, vol. 68, no. 3, pp. 1010–1016, Mar. 1990, doi: 10.1152/jappl.1990.68.3.1010.

[23] K. P. Strohl, J. Mead, R. B. Banzett, S. H. Loring, and P. C. Kosch, "Regional differences in abdominal muscle activity during various maneuvers in humans," *J. Appl. Physiol.*, vol. 51, no. 6, pp. 1471–1476, Dec. 1981, doi: 10.1152/jappl.1981.51.6.1471.

[24] A. Ratnovsky, D. Elad, and P. Halpern, "Mechanics of respiratory muscles," *Respir. Physiol. Neurobiol.*, vol. 163, no. 1, pp. 82–89, 2008, doi: https://doi.org/10.1016/j.resp.2008.04.019.

[25] A. Villoria, F. Azpiroz, A. Soldevilla, F. Perez, and J.-R. Malagelada, "Abdominal accommodation: A coordinated adaptation of the abdominal wall to its content," *Amer. J. Gastroenterol.*, vol. 103, no. 11, pp. 2807–2815, 2008.

[26] J. M. Goldman, L. S. Rose, M. D. Morgan, and D. M. Denison, "Measurement of abdominal wall compliance in normal subjects and tetraplegic patients," *Thorax*, vol. 41, no. 7, pp. 513–518, Jul. 1986, doi: 10.1136/thx.41.7.513.

[27] K. J. Cho, S. Y. Lee, and M. G. Brown, "Acupressure device," U.S. Patent 10117805B2, Nov. 6, 2018.

[28] K. J. Cho, S. Y. Lee, and M. G. Brown, "Acupressure device assisting breath," KR1020140037952A, Sep. 29, 2016.

[29] R. A. McBain, C. L. Boswell-Ruys, B. B. Lee, S. C. Gandevia, and J. E. Butler, "Abdominal muscle training can enhance cough after spinal cord injury," *Neurorehabil. Neural Repair*, vol. 27, no. 9, pp. 834–843, Jul. 2013, doi: 10.1177/1545968313496324.

[30] H. I. Krebs *et al.*, "Rehabilitation robotics: Performance-based progressive robot-assisted therapy," *Auton. Robots*, vol. 15, no. 1, pp. 7–20, Jul. 2003, doi: 10.1023/A:1024494031121.

[31] M. Mihelj, T. Nef, and R. Riener, "A novel paradigm for patient-cooperative control of upper-limb rehabilitation robots," *Adv. Robot.*, vol. 21, no. 8, pp. 843–867, Jan. 2007, doi: 10.1163/156855307780851975.

[32] S. Y. Lee, U. Jeong, and K. J. Cho, "An application of user-friendly control for a respiratory rehabilitation and assistance robot," in *Proc. IEEE Int. Conf. Adv. Intell. Mechatron.*, Jul. 2015, pp. 441–446, doi: 10.1109/AIM.2015.7222573.

[33] Y. Zheng *et al.*, "Unobtrusive sensing and wearable devices for health informatics," *IEEE Trans. Biomed. Eng.*, vol. 61, no. 5, pp. 1538–1554, May 2014, doi: 10.1109/TBME.2014.2309951.

[34] M. Sedláček and M. Krumpholc, "Digital measurement of phase difference—A comparative study of DSP algorithms," *Metrol. Meas. Syst.*, vol. 12, no. 4, pp. 427–448, 2005.

[35] M. Sedláček, "Digital measurement of phase difference of LF signals—A comparison of DSP algorithms," in *Proc. 27th IMEKO World Congr.*, 2003, pp. 639–644.

[36] D. Govin, L. Saenz, G. Athanasaki, L. Snyder, and P. Polygerinos, "Design and development of a soft robotic back orthosis," in *Proc. Des. Med. Devices Conf.*, 2018, Art. no. V001T10A001.

[37] I. L. Kron, P. K. Harman, and S. P. Nolan, "The measurement of intra-abdominal pressure as a criterion for abdominal re-exploration," *Ann. Surg.*, vol. 199, no. 1, pp. 28–30, Jan. 1984, doi: 10.1097/00000658-198401000-00005.

[38] A. G. Cresswell, H. Grundström, and A. Thorstensson, "Observations on intra-abdominal pressure and patterns of abdominal intra-muscular activity in man," *Acta Physiologica Scandinavica*, vol. 144, no. 4, pp. 409–418, Apr. 1992, doi: 10.1111/j.1748-1716.1992.tb09314.x.

[39] S. Sykora, "Approximations of ellipse perimeters and of the complete elliptic integral E(x)," Review of known formulae Stan's Library, 2005.

[40] M. Verhaegen and V. Verdult, *Filtering and System Identification: A Least Squares Approach*. Cambridge, U.K.: Cambridge Univ. Press, 2007.

[41] P. Ghafarian, H. Jamaati, and S. M. Hashemian, "A review on human respiratory modeling," *Tanaffos*, vol. 15, no. 2, pp. 61–69, 2016.

[42] E. Saatçi, E. Saatci, and A. Akan, "Analysis of linear lung models based on state-space models," *Comput. Methods Programs Biomed.*, vol. 183, 2020, Art. no. 105094.

[43] F. Vicario, A. Albanese, N. Karamolegkos, D. Wang, A. Seiver, and N. W. Chbat, "Noninvasive estimation of respiratory mechanics in spontaneously breathing ventilated patients: A constrained optimization approach," *IEEE Trans. Biomed. Eng.*, vol. 63, no. 4, pp. 775–787, Apr. 2016.

[44] J. H. Bates and G. B. Allen, "The estimation of lung mechanics parameters in the presence of pathology: A theoretical analysis," *Ann. Biomed. Eng.*, vol. 34, no. 3, pp. 384–392, 2006.

[45] J. H. Bates and B. Suki, "Assessment of peripheral lung mechanics," *Respir. Physiol. Neurobiol.*, vol. 163, no. 1–3, pp. 54–63, 2008.

[46] S. Khirani *et al.*, "On-line monitoring of lung mechanics during spontaneous breathing: A physiological study," *Respir. Med.*, vol. 104, no. 3, pp. 463–471, 2010.

[47] G. Avanzolini, P. Barbini, A. Cappello, and G. Cevenini, "Real-time tracking of parameters of lung mechanics: Emphasis on algorithm tuning," *J. Biomed. Eng.*, vol. 12, no. 6, pp. 489–495, 1990.

[48] C. Schranz, P. D. Docherty, Y. S. Chiew, K. Möller, and J. G. Chase, "Iterative integral parameter identification of a respiratory mechanics model," *Biomed. Eng. Online*, vol. 11, no. 1, pp. 1–14, 2012.
[49] G. Tonietti, R. Schiavi, and A. Bicchi, "Design and control of a variable stiffness actuator for safe and fast physical human/robot interaction," in *Proc. IEEE Int. Conf. Robot. Automat.*, 2005, pp. 526–531.
[50] D. Braun, M. Howard, and S. Vijayakumar, "Optimal variable stiffness control: Formulation and application to explosive movement tasks," *Auton. Robots*, vol. 33, no. 3, pp. 237–253, 2012.
[51] F. Ferraguti, C. Secchi, and C. Fantuzzi, "A tank-based approach to impedance control with variable stiffness," in *Proc. IEEE Int. Conf. Robot. Automat.*, 2013, pp. 4948–4953.
[52] A. Athanasiades *et al.*, "Energy analysis of a nonlinear model of the normal human lung," *J. Biol. Syst.*, vol. 8, no. 02, pp. 115–139, 2000.
[53] H. Lorino, A.-M. Lorino, A. Harf, G. Atlan, and D. Laurent, "Linear modeling of ventilatory mechanics during spontaneous breathing," *Comput. Biomed. Res.*, vol. 15, no. 2, pp. 129–144, 1982.
[54] A. Jafari, M. Nabeel, and J.-H. Ryu, "The input-to-state stable (ISS) approach for stabilizing haptic interaction with virtual environments," *IEEE Trans. Robot.*, vol. 33, no. 4, pp. 948–963, Aug. 2017.
[55] E. D. Sontag, "Smooth stabilization implies coprime factorization," *IEEE Trans. Autom. Control*, vol. 34, no. 4, pp. 435–443, Apr. 1989.
[56] E. D. Sontag, "Input to state stability: Basic concepts and results," in *Nonlinear and Optimal Control Theory*. Berlin, Germany: Springer, 2008, pp. 163–220.
[57] E. D. Sontag and Y. Wang, "On characterizations of the input-to-state stability property," *Syst. Control Lett.*, vol. 24, no. 5, pp. 351–359, 1995.
[58] H. K. Khalil, *Nonlinear Control*. New York, NY, USA: Pearson Higher Education, 2014.
[59] E. Sontag and A. Teel, "Changing supply functions in input/state stable systems," *IEEE Trans. Autom. Control*, vol. 40, no. 8, pp. 1476–1478, Aug. 1995.
[60] M. Vitacca *et al.*, "Breathing pattern and respiratory mechanics in patients with amyotrophic lateral sclerosis," *Eur. Respir. J.*, vol. 10, no. 7, Jul. 1997, Art. no. 1614.
[61] M. C. Apps, P. C. Sheaff, D. A. Ingram, C. Kennard, and D. W. Empey, "Respiration and sleep in Parkinson's disease.," *J. Neurol. Neurosurgery, Psychiatry*, vol. 48, no. 12, Dec. 1985, Art. no. 1240, doi: 10.1136/jnnp.48.12.1240.
[62] *Assisted Coughing : A Guide for Patients and Carers*. Amsterdam, The Netherlands: Physiotherapy Department of Buckinghamshire Healthcare NHS Trust, Buckinghamshire Healthcare NHS Trust, 2018.
[63] D. Frownfelter and E. Dean, "Facilitating airway clearance with coughing techniques," in *Cardiovascular and Pulmonary Physical Therapy: Evidence to Practice*. Amsterdam, The Netherlands: Elsevier, 2021.
[64] J. R. Bach and L. R. Saporito, "Criteria for extubation and tracheostomy tube removal for patients with ventilatory failure: A different approach to weaning," *Chest*, vol. 110, no. 6, pp. 1566–1571, Dec. 1996, doi: 10.1378/chest.110.6.1566.
[65] C. H. Taal, R. C. Hendriks, R. Heusdens, and J. Jensen, "An algorithm for intelligibility prediction of time–frequency weighted noisy speech," *IEEE Trans. Audio, Speech, Lang. Process.*, vol. 19, no. 7, pp. 2125–2136, Sep. 2011, doi: 10.1109/TASL.2011.2114881.
[66] O. Lartillot, T. Eerola, P. Toiviainen, and J. Fornari, "Multi-feature modeling of pulse clarity: Design, validation and optimization," in *Proc. 9th Int. Conf. Music Inf. Retrieval*, 2008, pp. 521–526.
[67] P. Boersma and D. Weenink, "PRAAT—A system for doing phonetics by computer," *Glot Int.*, vol. 5, pp. 341–345, Jan. 2001.

Sang-Yoep Lee (Member, IEEE) received the B.S. and Ph.D. degrees in mechanical and aerospace engineering from the Seoul National University, Seoul, South Korea, in 2014 and 2021, respectively.

He is currently with the Soft Robotics Research Center, Seoul National University. His research interests include soft/wearable robotics, medical/rehabilitation robotics, biomedical engineering, human–robot interaction, robot control/programming, algorithms, mechatronics, biomechanics, and user-centered design.

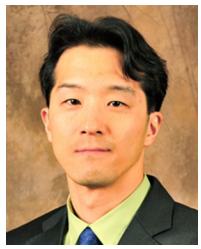

Jin-Oh Hahn (Senior Member, IEEE) received the B.S. and M.S. degrees in mechanical engineering from the Seoul National University, Seoul, South Korea, in 1997 and 1999, respectively, and the Ph.D. degree in mechanical engineering from the Massachusetts Institute of Technology, Cambridge, MA, USA, in 2008.

He is currently with the University of Maryland, College Park, MD, USA, where he is currently an Associate Professor with the Department of Mechanical Engineering, a Fischell Fellow with the Robert E. Fischell Institute for Biomedical Devices, and a Faculty Affiliate with the Applied Mathematics, Statistics, and Scientific Computation Program. His research interests include applications of dynamical systems, control, and machine learning theory to health monitoring, fault diagnostics, maintenance, and treatment of dynamical systems with emphasis on health and medicine.

Dr. Hahn was a recipient of the Young Investigator Grant Award from the Korean–American Scientists and Engineers Association, in 2013, the Young Investigator Program Award from the Office of Naval Research, in 2014, the Best BioSystems and Healthcare Paper Award from the Bio-Systems and Healthcare Technical Committee in the Dynamic Systems and Control Division of ASME, in 2017, the Faculty Early Career Development (CARRER) Award from the National Science Foundation, in 2018, IEEE EMBS Most Impactful Paper Award from the IEEE Engineering in Medicine and Biology Society, in 2019, and the Outstanding Gemstone Mentor Award from the Gemstone Honors Program at the University of Maryland, in 2019. He is an Associate Editor of the *ASME Journal of Dynamic Systems, Measurement and Control*.

Jaewon Beom received the M.D., M.M.Sc. degrees in clinical medicine from the college of medicine, Seoul National University, Seoul, South Korea, in 2004 and 2011, respectively, and the Ph.D. degree in biomedical engineering from the college of medicine, Seoul National University, Seoul, South Korea, in 2016.

He is currently a Clinical Professor with the Department of Rehabilitation Medicine, Seoul National University College of Medicine, Seoul National University Bundang Hospital. His research interests include medical robotics, patient rehabilitation, biomechanics, and neuromuscular disorders.

Ji-Hong Park received the M.D. degree in clinical medicine from the College of Medicine, Seoul National University, Seoul, South Korea, in 2010.

He is currently a Clinical Professor with the Department of Rehabilitation Medicine, Seoul National University College of Medicine, Seoul National University Bundang Hospital. His research interests include neurorehabilitation and sonography.

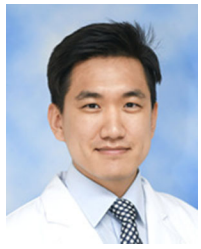

Han Eol Cho received the M.D. degree in clinical medicine from the college of medicine, Yonsei University, Seoul, South Korea, in 2011.

He is currently a Clinical Research Fellow with the Department of Rehabilitation Medicine, Yonsei University. His research interests include neuromuscular diseases, management of ventilatory insufficiency, machine-learning-based prediction of disease, pulmonary function evaluation, and noninvasive ventilators.

Seong-Woong Kang recieved the M.D. degree in clinical medicine from the college of medicine, Yonsei University, Seoul, South Korea, in 1985, and the M.M.Sc. and Ph.D. degrees in rehabilitation medicine from the college of medicine, Yonsei University, Seoul, South Korea, in 1991 and 1996, respectively.

He is currently a Professor of Rehabilitation Institute of Neuromuscular Disease, Yonsei University College of Medicine and Department of Rehabilitation Medicine, Gangnam Severance Hospital, and the Director of the Pulmonary Rehabilitation Center. He is also a Visiting Professor with the Padjadjaran University, Bandung, Indonesia. He is currently an Advisory Physician with the Korea ALS Association, a Medical Advisory Committee in the National Pension Review Board, a member of National Academy of Medicine of Korea, a Chairman of Congress committee in the Asia-Oceanian Society of Physical and Rehabilitation Medicine, a Director of Korean Academy of Geriatric Rehabilitation Medicine, and a Committee Member in the Ministry of Health and Welfare, Expert Committee of Rare Disease.

Prof. Kang was the recipient of the 2003 Academic Award from Korean Academy of Rehabilitation Medicine, 2013 Commendation from the Minister of Health and Welfare (support for patients with rare and incurable diseases), 2016 Commendation from Minister of Health and Welfare (support for patients with rare and incurable diseases), 2017 Hanmi Inspiratory Medical Professional Award from Hanmi Pharm jointly with Seoul Medical Association (dedication to rare and incurable diseases), and 2019 Service Merit Medal from Republic of Korea. He was an Editorial Board Member of the *European Journal of Physical and Rehabilitation Medicine* from 2012 to 2015, an International Advisory Board member in the *Indian Journal of Physical Medicine and Rehabilitation* from 2017 to 2019, and has been an International Editor in the *Chinese Journal of Rehabilitation Medicine* since 2015.

Kyu-Jin Cho (Member, IEEE) received the B.S. and M.S. degrees in mechanical engineering from the Seoul National University, Seoul, South Korea, in 1998 and 2000, respectively, and the Ph.D. degree in mechanical engineering from the Massachusetts Institute of Technology, Cambridge, MA, USA, in 2007.

He was a Postdoctoral Fellow with the Harvard Microrobotics Laboratory, Cambridge, MA, USA, until 2008. He is currently a Professor of Mechanical Engineering and the Director of the Biorobotics Laboratory and Soft Robotics Research Center, Seoul National University. His research interests include biologically inspired robotics, soft robotics, soft wearable devices, novel mechanisms using smart structures, and rehabilitation and assistive robotics.

Prof. Cho was the recipient of the 2014 IEEE RAS Early Academic Career Award, 2014 ASME Compliant Mechanism Award, 2013 IROS Best Video Award, and 2013 KSPE Paik Am Award.